DATA ACQUISITION SYSTEM FOR PHOTOACOUSTIC TECHNIQUE

M.Tech. Thesis

By

MRADUL MAURYA

DEPARTMENT OF ELECTRICAL ENGINEERING

INDIAN INSTITUTE OF TECHNOLOGY INDORE

JUNE 2022

DATA ACQUISITION SYSTEM FOR PHOTOACOUSTIC TECHNIQUE

A THESIS

Submitted in partial fulfillment of the requirements for the award of the degree

of

Master of Technology

by

MRADUL MAURYA

DEPARTMENT OF ELECTRICAL ENGINEERING

INDIAN INSTITUTE OF TECHNOLOGY INDORE

JUNE 2022

INDIAN INSTITUTE OF TECHNOLOGY INDORE

CANDIDATE'S DECLARATION

I hereby certify that the work which is being presented in the thesis entitled **DATA ACQUISITION SYSTEM FOR PHOTOACOUSTIC TECHNIQUE** in the partial fulfillment of the requirements for the award of the degree of **MASTER OF TECHNOLOGY** and submitted in the **DEPARTMENT OF ELECTRICAL ENGINEERING, Indian Institute of Technology Indore**, is an authentic record of my own work carried out during the time period from August 2020 to May 2022 under the supervision of Dr. Srivathsan Vasudevan, Associate Professor, Department of Electrical Engineering, IIT Indore.

The matter presented in this thesis has not been submitted by me for the award of any other degree of this or any other institute.

30/05/22

Signature of the student with date
MRADUL MAURYA

This is to certify that the above statement made by the candidate is correct to the best of my knowledge.

30/5/22

Signature of the Supervisor of
M.Tech. thesis #1 (with date)
Dr. SRIVATHSAN VASUDEVAN

MRADUL MAURYA has successfully given his M.Tech. Oral Examination held on **7th June 2022.**

7/6/22

Signature of Supervisor of M.Tech. thesis
Date:

Convener, DPGC
Date: 07/06/2022

Signature of PSPC Member #1
Date: 07/06/2022

Signature of PSPC Member #2
Date: 09/06/2022

ACKNOWLEDGEMENTS

I would like to express my gratitude towards my faculty advisor, Dr. Srivathsan Vasudevan, Asso. Prof., Department of Electrical Engineering, IIT Indore, for being supportive, always entertaining my queries and being completely involved in the project. His immense knowledge and patience guided me through the walks of my research and in writing this thesis.

I also extend my heartiest thanks to my project PSPC members: Dr. Swaminathan Ramabadran and Dr. Anjan Chakraborty for their encouragement and insightful comments and also for putting up tough questions which helped me to widen my research perspectives.

I would also like to thank Mr. Suhel Khan, PhD scholar, Department of Electrical Engineering, IIT Indore, for helping me conduct experiments on his custom-made laser excitation system for photoacoustic imaging experiments. In addition to that, he was very supportive and maintained a healthy work environment, which allowed me to work in my full efficiency.

I could not have imagined completing my project and thesis without the constant insight and support of my friends.

My heartfelt gratitude goes to my parents, who made all the sacrifices on my behalf, especially for their support and understanding. They have always been a source of inspiration and motivation for me throughout my life.

Dedicated to my family

Abstract

With medical technology advancing at a rapid rate, improving the portability and mobility of biomedical instruments adds an extra advantage. The end-user would also desire the instrument to be easily manageable and simple to learn. To address these issues, a portable, low-cost and compact data acquisition system has been developed in this thesis, to capture and store photoacoustic signals. Utilizing the photoacoustic effect, it is possible to differentiate between healthy and unhealthy tissues using the proposed DAQ system, by analysing the acquired photoacoustic signals.

A basic data acquisition system consists of a signal conditioning circuit, an ADC and a data displaying/analysing instrument. However, additional blocks may be added according to the desired application. The proposed DAQ includes a pre-amplifier to amplify the microvolt-PA signal, an ADC circuit to convert the analog PA signal into digital and finally a microcontroller to read, store, manipulate and transfer the data to the PC. Additional circuits to boost the trigger signal and to purify the microcontroller-generated clock for the ADC have also been designed.

The proposed DAQ has been incorporated in a custom-built laser diode-based excitation system to acquire photoacoustic signals in a PA imaging experimentation setup, to excite a black rubber sample. It was observed that the signal acquired using the proposed DAQ replicates the signal acquired using the traditional signal capturing instrument i.e., DSO.

The thesis discusses a detailed description of the proposed setup and its components, including the methodology used in developing the prototype circuits and PCBs for different functions and the results for the same, proving the functionality and accuracy of the proposed DAQ system.

TABLE OF CONTENTS

LIST OF FIGURES

LIST OF TABLES

ACRONYMS

ADC	*Analog to Digital Converter*
AR-PAM	*Acoustic Resolution Photo-Acoustic Microscopy*
BJT	*Bipolar Junction Transistor*
CE	*Common-Emitter*
CPC-P*x*	*Clock Purification Circuit – Prototype x*
CPU	*Central Processing Unit*
CT scan	*Computed Tomography scan*
DAQ	*Data Acquisition*
DC	*Direct Current*
DSO	*Digital Storage Oscilloscope*
EEG	*electroencephalogram*
EMI	*Electro-Magnetic Interference*
GPIO	*General Purpose Input/Output*
I2C	*Inter-Integrated Circuit*
KSPS	*Kilo-Samples Per Second*
LASER	*Light Amplification by Stimulated Emission of Radiation*
LCD	*Liquid Crystal Display*
LSB	*Least Significant Bit*
MRI	*Magnetic Resonance Imaging*
MSB	*Most Significant Bit*
MSPS	*Million Samples Per Second*
Nd-YAG	*Neodymium-doped Yttrium Aluminium Garnet*

OPO	*Optical Parametric Oscillator*
OR-PAM	*Optical Resolution Photo-Acoustic Microscopy*
PA	*Photo-Acoustic*
PACT	*Photo-Acoustic Computed Tomography*
PAI	*Photo-Acoustic Imaging*
PAM	*Photo-Acoustic Microscopy*
PAT	*Photo-Acoustic Tomography*
PC	*Personal Computer*
PCB	*Printed Circuit Board*
PET scan	*Positron Emission Tomography*
RPi	*Raspberry Pi*
RTD	*Resistance Temperature Detector*
SNR	*Signal to Noise Ratio*
SPI	*Serial Peripheral Interface*
SRAM	*Static Random Access Memory*
UART	*Universal Asynchronous Receiver-Transmitter*
USART	*Universal Synchronous/Asynchronous Receiver-Transmitter*

Chapter 1

Introduction and Literature Survey

1.1 Motivation and Objective

Medical diagnostics has always been an important part of treating simple as well as fatal diseases. When medical science and technology is advancing at an exponential rate, accurate diagnosis is not sufficient. Accuracy is a necessity, but along with accuracy, diagnosis methods and instruments need to be safe, quick, portable and cost-effective. Focus on diagnostic research over the last two decades has led to major developments and improvements in biomedical imaging systems. A typical biomedical imaging system comprises of various subsystems for performing specific tasks such as sensing, signal conditioning, acquisition, processing and accurate visualization of living or damaged tissues.

Among several biomedical imaging techniques, the photoacoustic technique has had some remarkable discoveries, resulting in the significant evolution of this technique over the last decade. When compared to other imaging techniques like CT scan, MRI, PET scan, etc., the photoacoustic technique is found to have high sensitivity and accuracy in diagnosis of various diseases. In addition to this, photoacoustic method uses non-ionizing radiation, which is completely safe unlike other techniques which use ionizing radiation.

The photoacoustic imaging technique is based on the photoacoustic effect. Due to this effect, when light is incident on a sample, sound waves are emitted [5]. Hence comes the name, 'photoacoustic'. Basically, photoacoustic (PA) imaging is detecting and analyzing ultrasonic (acoustic) emission resulting due to optical (pulsed laser) excitation [6]. Upon excitation on a biological tissue, the energy from the nanosecond laser pulses is converted to heat, which results in thermal expansion inside the tissue. That energy is released by the tissue in the form of acoustic (ultrasound) waves, which are then detected by an ultrasound sensor [7]. In order to form an accurate tomographic image, multiple ultrasound detectors and DSOs must be carefully positioned around the sample. Furthermore, the signal from the ultrasound detector will need to be passed through a signal conditioning circuit before it can be seen on a DSO. Including all these instruments and stages makes the system bulky and cumbersome, while also increasing the overall cost of the system. Although photoacoustic imaging offers numerous advantages in biomedical applications, this technique is yet to be commercialized in the clinical field. Much research, data collection and field testing are essential before PA imaging can be viewed as an alternative for accurate medical diagnosis.

The main aim of the project described in this thesis, is to take a step forward in the clinical research and development of a photoacoustic imaging system. This is done by designing and developing an accurate, compact, portable and cost-effective data acquisition system for capturing, storing, processing and analyzing photoacoustic signals. The developed DAQ system has been tested for all kinds of signals. The detailed description of all the components of the DAQ and the results obtained using the developed system are described in this thesis.

1.2 Photoacoustic Effect

Photoacoustic biomedical imaging is based on the photoacoustic effect. Due to this effect, when light is incident on a sample, sound waves are emitted. For this phenomenon to happen, the light must be modulated or pulsed, which means it should vary periodically. In biomedical applications, the light is in the form of pulsed laser, the sample can be any biological tissue and the emitted signal is in the form of ultrasound waves. The sample on which the laser is incident absorbs the incoming energy from the laser. This energy, after converting into kinetic energy, induces random motion and collisions inside the sample. This results in heating, which in turn results in thermal expansion of the sample. When the sample relaxes, this absorbed energy is dissipated in a non-radiative way in form of pressure waves or acoustic waves.

For the detection of the emitted ultrasonic waves, the transducer that is used is an ultrasound sensor. This sensor detects the ultrasound waves emitted from the sample and converts it into an electrical signal. This electrical signal is what is called in common terms, a photoacoustic or PA signal. The PA effect and imaging technique is depicted in Fig. 1.2. The details of the optical source, absorption, PA generation and detection are elaborated in the following sections.

1.2.1 PA wave generation

Alexander Graham Bell in 1880, discovered a phenomenon. He observed that when modulated light is shined upon certain substances, sound waves are emitted, the pitch of which depends upon the frequency of the vibratory change in light [13]. Since the incidence of light produced sound waves, this phenomenon was named the photoacoustic effect ('photo' means light and 'acoustic' means sound).

To produce a photoacoustic signal, following are the necessary conditions to be fulfilled: -

- The incident light should be either modulated or pulsed.
- The wavelength of the incident light must be within optical absorption spectrum of the targeted sample' chromophores.
- If pulsed laser is incident, the pulse width should not exceed a few nanoseconds.

If all the above conditions are met, one should be able to observe the photoacoustic effect. The width of the pulse is decided according to the sample the light is incident onto. The pulse width should be lesser than the thermal relaxation time and stress relaxation time of the tissue. Generally, that value comes out be around 5-10 ns [14].

1.2.2 PA wave propagation and detection

The ultrasound waves generated from the sample will need to be propagated to the detector. Before reaching the detector, the waves propagate through a coupling medium. Any medium can be used to couple the sample and the detector, but the signal intensity depends upon the dielectric coefficient of the coupling medium. Water and ultrasound gel are commonly used coupling mediums. After the waves propagate through the medium, they are finally detected by the ultrasound sensor/detector, which then converts those waves into an electrical signal, which is finally called a photoacoustic or PA signal.

Fig. 1.1 illustrates the generation, propagation and detection of a photoacoustic wave. Laser is incident upon the sample, which results in thermal expansion of the tissue. When the tissue relaxes, the released energy generates acoustic waves, which are then detected by an ultrasound detector after propagation through a coupling medium.

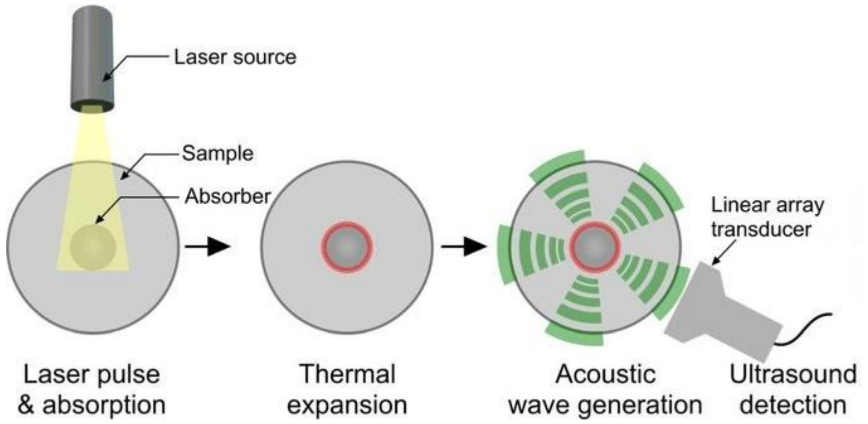

Fig. 1.1 – PA wave generation, propagation and detection [15]

1.3 Overview of the Photoacoustic Imaging Technique

The evolution of biomedical imaging techniques for medical diagnosis has enabled significant development in screening, detailed diagnosis and continuous monitoring of any pathological condition. Existing imaging techniques have evolved up to the point that healthy and unhealthy tissues can be distinguished easily with high precision and quality. Ideally, a medical imaging technique should have high contrast, resolution, penetration profile, etc.

When compared with other existing clinical imaging techniques, following are the advantages of photoacoustic imaging [8]: -

- High intrinsic optical absorption contrast compared to pure optical and pure ultrasonic techniques.
- Better penetration depth (0.1 to 12 cm) compared to other optical methods.
- Photoacoustic imaging is free from speckle artifacts unlike ultrasound imaging.

- This technique is compact, faster and cost-effective in comparison to MRI, PET scan and CT scan.
- Since it can be used in multiple wavelengths, this technique can provide both structural and functional information.
- Sensitivity is two orders of magnitude greater than those of confocal microscopy and optical coherence tomography.
- Multiscale multi-contrast images of biological structures can be obtained, ranging from organelles to organs.

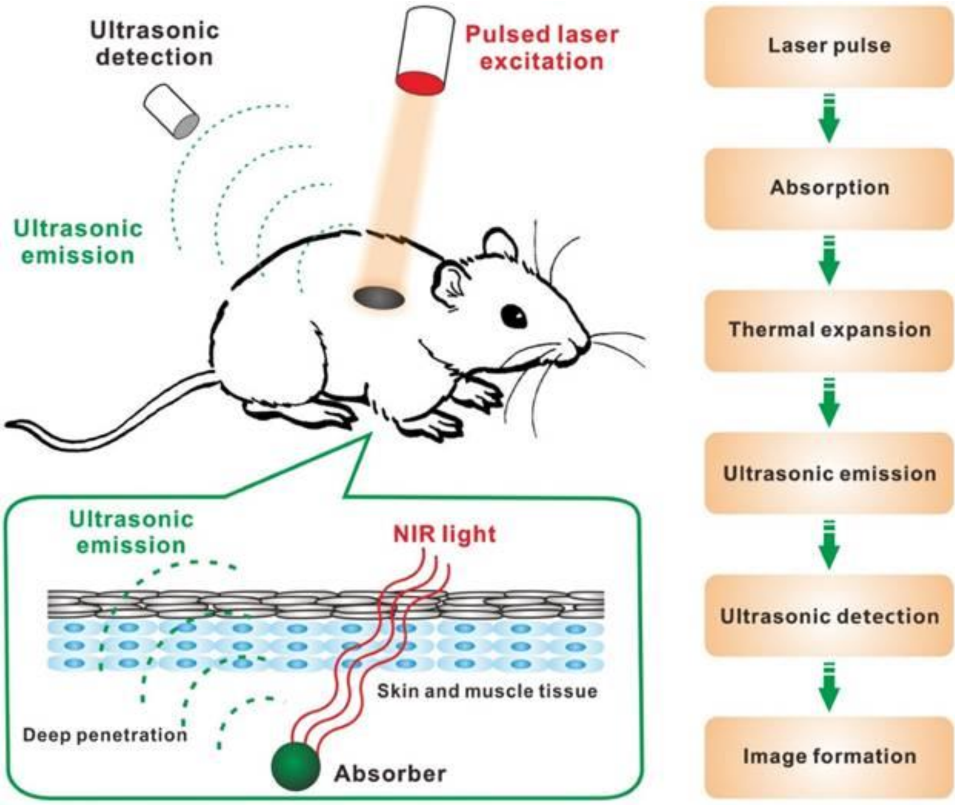

Fig. 1.2 – Schematic illustration showing the process of photoacoustic imaging [12]

Photoacoustic imaging, as the name suggests, is a mixture of both optical and non-optical (laser and ultrasound) techniques [9]. PA imaging has emerged as a technique possessing all the necessary characteristics needed for any bio-imaging modality, including high optical absorption contrast, non-ionizing radiation, sub-micrometer resolution, non-invasiveness, etc., that too, at penetration depths exceeding 5 cm [10,11].

The photoacoustic effect is caused by the optical excitation of any sample (tissue in biomedical applications). This excitation results in the emission of acoustic (ultrasound) waves from the sample. The amount of ultrasonic emission resulting from the laser excitation of tissue depends upon the optical absorption coefficient of hemoglobin, fats, melanin, water and other tissue chromophores [6]. The reason why this technique is superior is because it utilizes the high penetration depth of optical excitation and low scattering emission of acoustic waves.

1.4 Types of PA Techniques

Apart from imaging in the biomedical field, the photoacoustic technique also has applications in other fields. This technique has also been explored for applications in spectroscopy and signal analysis. Therefore, the PA technique is broadly divided into three applications, imaging, spectroscopy and signal analysis. Photoacoustic imaging is further subdivided into two categories, PA tomography and PA microscopy. Fig. 1.3 shows the typical classification of photoacoustic technique.

Photoacoustic computed tomography (PACT) has been extensively studied for the molecular imaging of living tissues using functional non-ionizing radiation. Usually, to penetrate deep inside the tissue, the laser which is used is either bulky or expensive or both. This creates a shortcoming of this technique. However, to overcome this issue, laser diodes have emerged as an alternative which is compact as well as cost-effective. The most commonly used lasers in PACT systems are Q-switched, nanosecond pulsed tunable lasers based on Nd:YAG (Neodymium-doped Yttrium Aluminium Garnet)/OPO (Optical Parametric Oscillator). For detection and data acquisition, multichannel ultrasound detector array with associated DAQ is used.

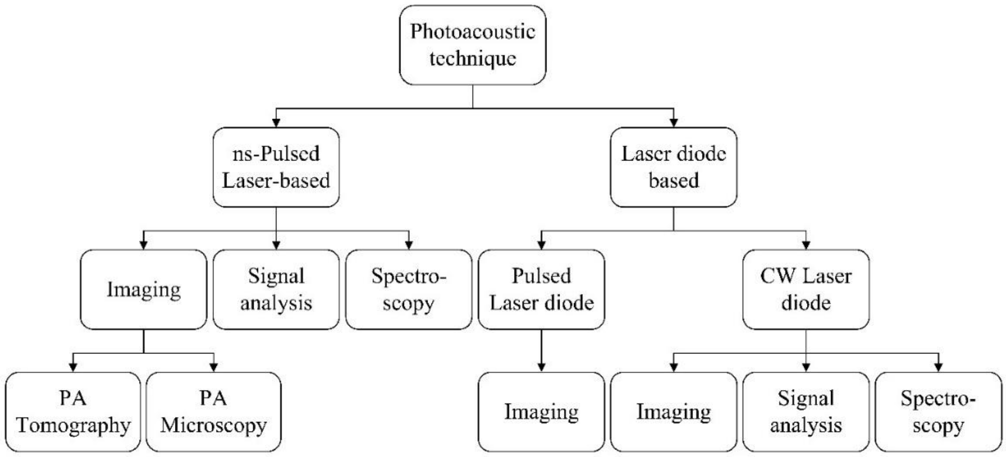

Fig. 1.3 – Classification of photoacoustic technique [35]

The most commonly used lasers in PACT systems are Q-switched, nanosecond pulsed tunable lasers based on Nd:YAG (Neodymium-doped Yttrium Aluminium Garnet)/OPO (Optical Parametric Oscillator). For detection and data acquisition, multichannel ultrasound detector array with associated DAQ is used. To achieve an adequate SNR of the PA signal, the lasers produce several hundreds of millijoules of laser pulse energy. This amount of energy ensures that the excited laser penetrates till several centimeters deep inside the tissue, such as the deep vasculature of a human breast. But these lasers are not clinically applicable. The two main reasons for this are its bulkiness and high cost. The energy created by these lasers is achieved by creating high-energy pulses with low repetition frequencies (< 20 Hz). However, an equal amount of energy can be generated by creating low-energy pulses with high repetition frequencies (> 1 KHz) using laser diodes. This has already been achieved by many researchers to create photoacoustic imaging systems using laser diodes.

1.4.1 PA Tomography

Photoacoustic Tomography (PAT) is the fundamental technique in the field of biomedical imaging. It may also be referred to as optoacoustic/thermoacoustic tomography. It uses nano-second pulses of laser to excite the sample, to which acoustic waves are propagated in response from the sample. To collect these emitted acoustic waves, multiple transducers must be placed all around the sample to collect signals from all directions. Alternatively, a single transducer can be revolved around the sample to collect the PA signals from all directions.

The former technique requires more hardware and is therefore complex and expensive. The latter one is time-consuming and requires repetitive heating of the sample. When using multiple transducers, the geometry of the array to place the transducers is chosen and created according to the corresponding geometry of the sample. Finally, all the photoacoustic signals from all directions are combined to generate the final image using reconstruction algorithms.

1.4.2 PA microscopy

Among all the photoacoustic techniques, PA microscopy is the only technique which allows us to visualize blood vessels at sub-micrometer scale. In PAM, a single element ultrasound transducer is scanned around the sample to generate the image. Alternatively, the ultrasound transducer may be fixed while the directed laser beam is scanned alongside the sample. PA microscopy is further subcategorized as optical-resolution photoacoustic microscopy (OR-PAM) and acoustic-resolution photoacoustic microscopy (AR-PAM), based on the scanning mechanism [18]. The relative size of the ultrasonic or optical focus determines the lateral resolution, while the axial resolution is determined by the time-resolved photoacoustic signal [19]. PA microscopy, along with its use in detailed imaging, can also be used for image-guided surgery and treatment. However, since the image resolution and penetration depth are scalable, the penetration depth is restricted in order to achieve sub-micrometre resolution.

1.5 Introduction to Data Acquisition System

Acquiring data has been one of the most important and basic tasks in any experiment or analysis. Manual data writing is the traditional method of data acquisition. In fact, this was the only method used in earlier times to analyse and device or instrument. But with the rapid advancement of technology, this method is becoming obsolete and impractical, especially in systems working on high frequencies, which require rapid data collection, management and analysis. Thus, the need for a DAQ. A data acquisition system is a collection of hardware and software which allows the user to collect, store and analyse the physical data from the real world. It may use a sensor/transducer to convert the physical data into electrical signal, amplifiers and filters for signal conditioning, an ADC to convert this data into digital, which can then be read and analysed on a PC or any other display/analysis instrument. Over the last decade, the use of DAQs for data collection, control and analysis has revolutionized modern-day science, production and manufacturing. DAQ plays a vital role in bridging the gap between the physical world and the modern digital world.

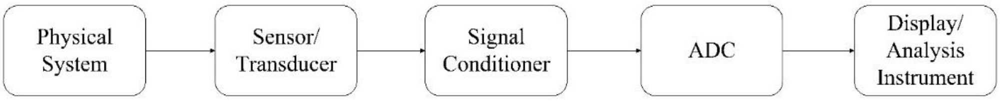

Fig. 1.4 – Basic DAQ block diagram

Figure 1.4 shows a typical DAQ block diagram. The first block depicts the physical system to be analyzed. It is crucial to know the nature of the physical data to be captured. This data cannot directly be measured. To convert this data into a measurable form, a sensor/transducer is used. A transducer is a device which converts energy from one form to another. In our application, the physical data in terms of waves, heat, light, pressure, etc. is converted to an electrical voltage signal by the transducer. However, most of the times, this voltage signal also requires one or more signal conditioning steps. This may include amplification, shaping or filtering. Signal conditioning ensures that the signal is within the tuning range of the ADC, while also protecting it against overvoltage and overcurrent from the signal. The ADC then digitizes the signal to a pre-defined resolution and sampling frequency, so that it can be read by any digital instrument/controller. This digital controller, after some processing, sends the acquired data to the PC for further analysis.

Data acquisition systems are application-specific. This is because all systems work on different operating frequencies, input range and nature, supply voltage, etc. Thus, there are some parameters to consider before designing the DAQ, like maximum sampling frequency, number of channels, input range, ADC resolution, supply voltage, center frequency of filter, etc. DAQs with their subsystems like sensors, communication links, filters, preamplifiers, etc., have been demonstrated in various systems. An acoustic delay line module is proposed to improve the imaging quality and speed of low-cost photoacoustic tomography (PAT) system[1], Arduino-based low-cost data-logger system is designed for the monitoring PV system[2], implementation of low-cost acquisition technology in the field of vehicle engineering[3], virtual electronic system for measuring the EEG signals[4], etc.

Portability is another advantage of a compact DAQ, particularly in medical applications, enhancing system mobility while simultaneously reducing system complexity. A portable compact DAQ provides continuous and non-invasive monitoring of health parameters. In this thesis, a compact portable DAQ is designed for bio-medical applications using photoacoustic imaging techniques.

1.5.1 Ultrasound detector

Ultrasound transducers are basically devices that detect ultrasound (acoustic) waves and convert them into an electrical signal. The basic principle involved in the working of an ultrasound transducer is the piezoelectric effect. This effect is observed in certain special materials called the piezoelectric crystals. Due to this effect, when a piezoelectric crystal is mechanically deformed, the crystal produces a change in resistance and current. In ultrasound transducers, the mechanical deformity is caused by the pressure waves coming from the acoustic wave emission from any sample. This deformity is converted into an electrical signal (a PA signal in photoacoustic imaging application). The signal's amplitude depends on the pressure of the waves.

The mass of the crystal depends upon the application it has to be used for. This is because it is the mass of the crystal which decides the transducer's center frequency and bandwidth. The ultrasound sensor consists of five major components [16]: -

- Piezoelectric crystal – The mass and thickness of the crystal determines the resonant frequency of the ultrasound transducer.
- Positive and ground electrodes – The electrodes allow for electrical connection. The positive electrode is connected on the back of the element and the ground electrode on the front.
- Damping (backing) block – This is adhered behind the positive electrode. The purpose of this block is to absorb the ultrasound energy directed backward and attenuate stray ultrasound signal from the housing.
- Matching layer – This is the interface between the transducer element and the tissue. Due to this layer, almost 100% transmission of the

ultrasound from the element into the tissues is achieved. This happens by minimizing reflection due to acoustic impedance mismatch.

- Housing – This includes a plastic case, metal shield and acoustic insulator to provide electrical insulation and protection of the element.

The above mentioned are the key components of an ultrasound transducer. The following section will discuss the signal conditioning of the PA signal.

1.5.2 Signal conditioning

The output signal from a sensor/transducer, in most cases, cannot be directly interfaced with the signal reading/display device. A signal conditioner takes an analog signal from a process sensor and converts it into a signal that is compatible with process monitoring and control devices. It is one of the most important components to any sensing system. Given the variance in signal strength and signal types from one analog sensor to another, without optimizing these signals, the accuracy of the sensors' measurements cannot be relied upon. Following are the different types of signal conditioning according to the need and application of a system: -

- Electrical isolation – Isolation helps to protect sensitive equipment from potential hazards that may come through the signal path from the sensor. The isolator can also filter out any unwanted noise along the signal path and eliminate any electrostatic interference caused by the ground loops which can also damage any devices that are connected to the sensor.
- Amplification – Amplification increases the input signal strength or amplitude with low voltage output sensors such as thermocouples and strain gauges. Amplification can increase the resolution of the measurement.
- Attenuation – It is the opposite of amplification. It is possible sometimes, that the range of the input signal exceeds the input limit of the ADC. In such cases, it is necessary to decrease the signal amplitude/strength in order to bring the signal within the detectable range. This type of conditioning is typically necessary when measuring voltages exceeding 10 V.

- Linearization – Linearization is necessary when sensors produce signals that are not linearly aligned to the physical measurement. This condition is common for thermocouple signals.
- Filtering – Not all of the signal frequency spectrum contains valid data. In fact, some frequencies like those in 50 Hz AC power lines can cause unwanted noise in the signal. That's where filtering is used to eliminate those unwanted frequencies for a clean and consistent signal.
- Excitation – Excitation voltage is required for the operation of an active sensor such as a thermistor, RTD or a pressure sensor. The stability and accuracy of the excitation signal directly affects the stability and accuracy of the sensor.
- Surge Protection – This is necessary in a circuit to protect the circuit against high voltage spikes that may accompany the signal.

Signal conditioning cannot be overlooked when designing a process measurement system. One or more of the above specified techniques can be used in any circuit according to the application.

1.5.3 Analog to Digital Conversion

In simple terms, an analog signal can be defined as a signal continuous with respect to time, whereas a digital signal is discrete with respect to time. While an analog signal has a value at every particular time, a digital signal has values at predefined instants which differ in time by one 'sampling interval'. Every signal present in the real world/environment is analog in nature. But in order to read and analyze these signals, we need to convert them into digital, otherwise any digital world device like the computer or a microprocessor would not be able to understand it. This conversion is achieved by devices known as ADCs (Analog to Digital Converters). ADCs are used to translate real world analog signals like pressure, temperature, distance, light intensity, etc. into its corresponding digital equivalent. After conversion, the signal can then be processed, computed, stored or transmitted [25].

The basic operation of an ADC is to convert an analog signal into a digital signal. This is achieved by sampling the analog signal at uniform intervals (depending on the sampling frequency of the ADC) and then assigning a digital value to each sample. This digital value appears on the output as an n-bit binary code (‘n’ being the resolution of the ADC). The digital value is obtained by dividing the sampled voltage by the reference voltage and then multiplying it by ‘n’. The analog to digital conversion process in simple words, is representing an analog signal which has infinite resolution, as a digital code that has finite resolution. Any sampled analog voltage will fall between any two of the quantization levels and according to the configuration, any one of those levels will be assigned to all the analog values falling between those two levels [25].

According to the need and application, ADCs are classified according to their specific architectures. Each architecture has its own pros and cons. Table 1.1 discusses the classification of analog to digital converters.

ADC Type	Pros	Cons	Max Resolution	Max Sample Rate	Main Applications
Successive Approximation (SAR)	Good speed/resolution ratio	No inherent anti-aliasing protection	18 bits	10 MHz	Data Acquisition
Delta-sigma (ΔΣ)	High dynamic performance, inherent anti-aliasing protection	Hysteresis on unnatural signals	32 bits	1 MHz	Data Acquisition, Noise and Vibration, Audio
Dual Slope	Accurate, inexpensive	Low Speed	20 bits	100 Hz	Voltmeters
Pipelined	Very fast	Limited resolution	16 bits	1 GHz	Oscilloscopes

Flash	Fastest	Low bit resolution	12 bits	10 GHz	Oscilloscopes

Table 1.1 – Classification of ADCs [26]

1.6 Photoacoustic Instrumentation

1.6.1 Conventional PA system

Fig. 1.5 shows a typical experimental setup for acquiring a single PA signal after laser excitation of a sample. For excitation of the sample, nano-second Nd: YAG pulsed laser is used. The laser irradiates the sample. This leads to a rise in temperature, which results in thermal expansion and thus generation of ultrasound waves. These ultrasound waves propagate through the coupling medium (water, for example) before they are detected by the ultrasound sensor and converted into a PA signal. Since only a single sensor is present here, it has to be revolved around the sample by small fixed angles to capture PA signals all around the sample. These signals are amplified and then digitized and transferred to the PC. In the PC, some further signal processing algorithms are run on the acquired data before the final tomographic image reconstruction. The quality of this image is dependent upon eight parameters, namely, detector view angle, element number, center frequency, bandwidth, aperture size, focusing, orientation error, and scan step angle error [24]. The reconstruction algorithm used in this study is based on single-variable analysis, which allows the change in only one parameter at a time, while keeping all others to be constant.

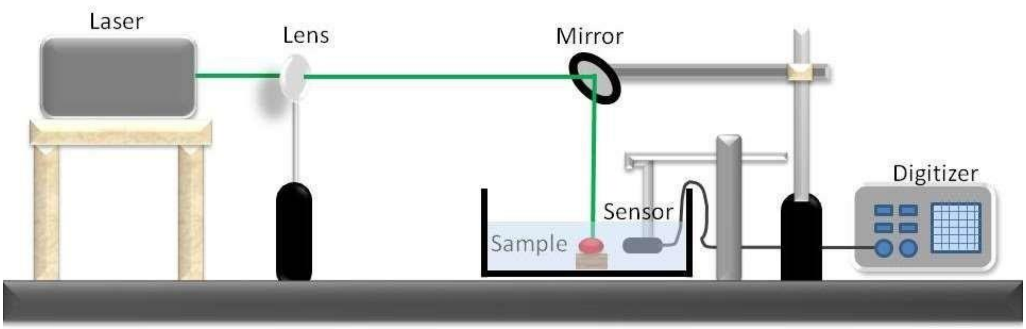

Fig. 1.5 – A typical photoacoustic sensing system

The photoacoustic systems based on a single ultrasound detector was very popular in early photoacoustic research studies. Even today, this setup is frequently used for studies requiring proof of concept in many experiments due to its effectiveness and simplicity. Due to use of a single sensor, imaging speed is high and cost is also low. However, for high-resolution imaging applications, multiple sensors will have to be used and carefully placed around the sample in order to collect PA signals and generate tomographic images. Fig. 1.6 illustrates the placements of multiple ultrasound detectors around the sample. The biggest challenge in employing multiple detectors is that we would need a separate DAQ for each particular ultrasound detector. This would increase the cost of the system and also make it bulky.

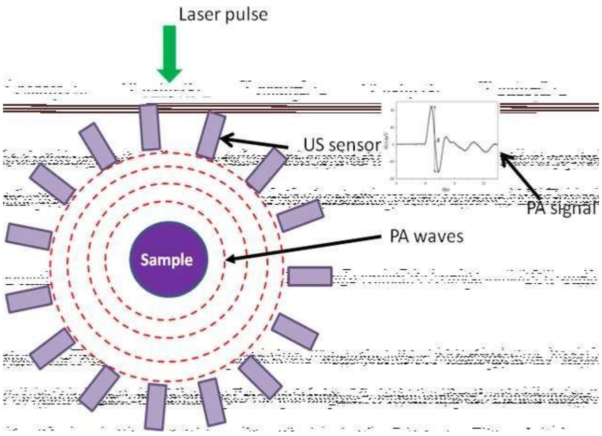

Fig. 1.6 – Placement of multiple sensors around the sample

1.6.2 Instrumentations for PAI

There are several companies who are working on photoacoustic imaging and developing instruments based on it. For the preclinical imaging of small animals, VisualSonics developed Vevo LAZR photoacoustic platform. This was however, based on ultrasound (US) imaging system. Apparently, in-vivo real time imaging offers both ease of control and whole-body imaging. Similar to VisualSonics, Endra Life Sciences manufactured Nexus 128 for diagnosis of cancer in small animals using photoacoustic imaging for preclinical uses. Along with this instrumentation, Endra Life Sciences also provides a built-in analysis software package which can generate high-resolution 2D and 3D photoacoustic images [20]. With the use of Nexus 128, Sompel et al. achieved an improvement of image quality of both tissues and phantoms. He achieved this by correcting temperature changes [21].

In addition to VisualSonics and Endra Life Sciences, iThera Medical and Seno

Medical Instruments have also developed their own photoacoustic instruments. They are termed MSOT (Multi-Spectral Optoacoustic Tomography) and LOUIS-3D respectively. Specifically designed for clinical applications, the MSOT Acuity included 2D and 3D detectors along with a fast-tunable 50 Hz laser. This device has been proven to achieve true real-time biomedical and quantitative imaging of lesions in brain through tissue chromophore distribution and concentration [20]. Among the 2D and 3D detectors, the 2D detector is better at applications of lowering signal decrease and anatomical resemblance, while the 3D probe is useful in rapid imaging and visualization of superficial areas [22].

Furthermore, the Twente Group, in collaboration with ESAOTE Europe BV, developed a novel dual-imaging modality. They combined an ultrasound transducer array and a diode stack laser in a signal ultrasound probe. This probe was then connected to a commercially available ultrasound (US) system. This new modality utilizes the advantages and features provided by both photoacoustic and ultrasound imaging. The functional information is provided by PAI and the anatomical details are provided by US imaging [23].

Instrument	**Modality**	**Advantage**	**Application**
LAZR (VisualSonics)	Ultrasound-photoacoustic imaging integrated	Whole-body with sectional PAI options	Preclinical
Nexus 128 (Endra Life Sciences)	Photoacoustic imaging	Fast imaging and high-resolution 3D image reconstruction	Preclinical cancer detection
MSOT (iThera Medical)	Photoacoustic Tomography	Real-time, whole-body tomography with body navigations	Preclinical whole-body PAI especially cancer detection and brain imaging

LOUIS-3D (Tomo Wave Laboratories, Inc.)	Photoacoustic imaging with tunable laser switch	The first PAI scanner for SLN dye injection guidance	Preclinical and clinical studies on oncology, vascular angiography, hematology, etc.

Table 1.2 - Typical commercial PAI instrumentations for preclinical and clinical studies [20]

1.7 Existing DAQ Systems

DAQ systems have applications in almost all the domains in today's world. That is why, each of them possesses a particular set of specifications depending upon the application they are to be used for. Shuangbao et al. have developed a high-speed DAQ based on FPGA in order to continuously acquire data for long-time and steady-state operation. The key feature of this system is that it can sample data at a rate of up to 80 MSPS continuously for 1250 seconds [27]. But the system is still bulky and although the design cost is reduced compared to commercial DAQ systems like DSOs, there is still scope of reducing the cost by a much greater extent. Another Arduino DUE – based DAQ has been built by González et al. to be used in vehicular dynamics applications. The system allows for interfacing of different sensors and peripherals like SD card, accelerometer, LCD etc. communicating by SPI and I2C protocols. The ADC used in the system is multi-channeled at 12-bit resolution. Although the authors have successfully created a low-cost and portable DAQ, but the key disadvantage of this system is its extremely low acquisition rate (max. 2 KSPS at single channel operation) [30]. Dantsker et al. have also interfaced several sensors to a Beaglebone microcomputer, in order to collect, store and transmit the data from the huge number of sensors in small to mid-sized unmanned aerial vehicles. Although they have successfully managed to collect and log the data from all the sensors, the operating frequency of the developed device is just 100 Hz, which is a major shortcoming of this device with reference to this thesis project's requirement [33]. A high-speed data acquisition system has also been developed by Soto-Ocampo et al. for monitoring the condition of rotating machinery through vibration analysis. They have used a small Raspberry Pi microcomputer to interface with the vibration sensors. The data from these sensors passes through an external ADC (maximum conversion rate of 250 KSPS at 16-bit resolution) before being read by the GPIOs of RPi. They have also incorporated up to 4 channels, with a conversion rate of 35 KSPS at 4-channel operation. This system satisfies the condition of high resolution, the sampling frequency is also high compared to other systems, but it is still not enough for this thesis' application [34].

Similar to a data acquisition system, a data logger is another device used for capturing and capturing/logging data, and then using it for further analysis. Nhivekar et al. have developed a data logger for remote monitoring of environmental parameters like temperature and humidity. They have used an AVR-based 8-bit microcontroller, interfaced it with temperature and humidity sensors. The data of these sensors are logged at pre-specified time intervals, stored in an SD card and also sent as an SMS to the user's mobile phone. They have successfully built a working data logging system, but there are a few shortcomings to it. Firstly, the microprocessor they are using works on a relatively low clock rate of 8-16 MHz. The internal ADC used is of 10-bit resolution at a maximum conversion rate of 15 KSPS [31]. Another data logger developed by Gakopoulos et al. captures the interaction between the wheelchair and its user. The sensor data is passed through a signal conditioning circuit before it is read by an AVR-based 8-bit microcontroller. That data is then stored in an SD card and then transmitted via Bluetooth for further analysis [32]. Although the system built by the authors is suitable for their application, the specifications of the microcontroller (16 MHz clock frequency) and ADC (maximum conversion rate of 15 KSPS at 10-bit resolution) does not meet the requirements of this thesis project.

It is worth noting that although the existing DAQ systems are able to interface with multiple sensors, incorporate signal conditioning circuits and also transfer data through wired or wireless communication, but fail to acquire signal data in the MHz range. This is a major challenge that has been tackled in this thesis project while simultaneously not compromising any of the other requirements of a DAQ system.

1.8 Organization of the Thesis

The entire work done for this thesis project has been explained in a total of four chapters: -

1. Chapter 1 introduces the basics of photoacoustic imaging, data acquisition systems and also the motivation and objective behind this project. Literature survey has also been done to gain knowledge about existing PA instrumentation and DAQ systems.
2. Chapter 2 provides a detailed insight into the novel work done for developing our own DAQ system for acquisition of photoacoustic signals.
3. Chapter 3 is dedicated for discussion and results. Results of all the developed blocks of the system have been shown and discussed thoroughly and finally successful acquisition of photoacoustic signals has been done and the results for the same have been discussed.
4. Chapter 4 concludes the work done for this thesis project and also discusses the scope of this project in the future.

Chapter 2

Design and Development of DAQ

This chapter discusses the detailed progress towards building a novel data acquisition system for acquiring photoacoustic signals.

2.1 Proposed DAQ System

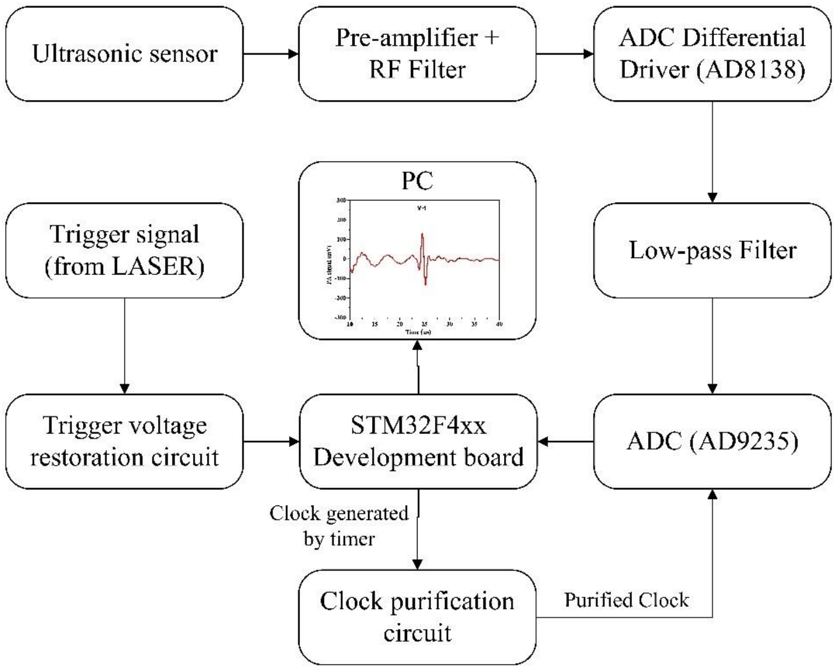

Fig. 2.1 – Proposed data acquisition system

The block diagram of the proposed low-cost, high-speed data acquisition system is shown in Fig. 2.1. The two main issues in acquiring photoacoustic signals are its amplitude and frequency. A typical photoacoustic signal lies in the 3-20 MHz spectrum and has amplitude in the range of few microvolts. The DAQ proposed in this thesis not only deals with these two key issues, but also provides other advantages including compactness, low-cost and feasibility in incorporating multiple sensors.

The photoacoustic signal is first passed through a two-stage CE amplifier to amplify the signal. This amplified signal is then passed through the ADC module, which includes the ADC differential driver, low pass filters and the ADC itself. The ADC converts the analog signal into its digital equivalent. This signal is then sent to the microcontroller, which synchronously captures the data multiple times according to the trigger signal frequency. The microcontroller is also used to generate the clock required for the functioning of the ADC, which is first purified before it reaches the ADC. After some internal processing in the microcontroller, the signal is sent via UART communication to the PC for display.

2.2 Pre-Amplifier

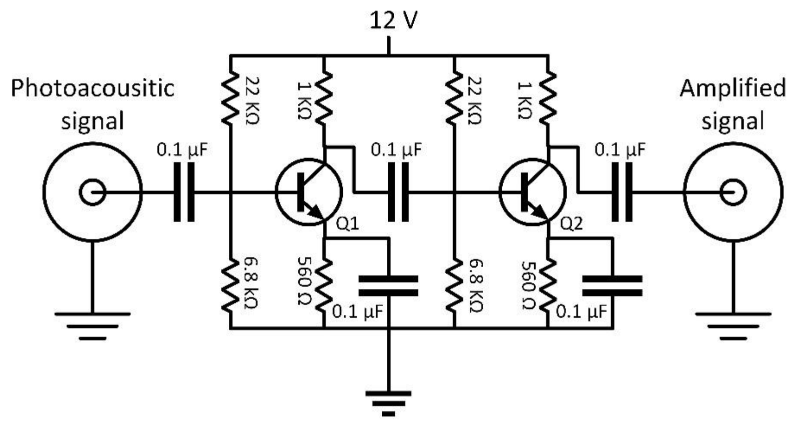

Fig. 2.2 – Pre-amplifier circuit diagram

As discussed in the previous sections, the amplitude of PA signals is in the range of tens of microvolts. It is practically impossible for any ADC to read a signal with such small amplitude. Thus, the need to amplify the signal. The most basic way to amplify a signal is to use a BJT in common-emitter (CE) configuration. Vasudevan et al. have designed and developed a three-stage amplifier circuit for amplifying photoacoustic signals for biomedical applications. The amplifier has been designed to provide a gain of approximately 80 dB. The first two stages are CE-configuration stages using BJT and the third stage is an operational amplifier. [35]. In the design proposed in this thesis, the third stage is omitted to eliminate the need of a -12V supply. This results in the operation of the entire DAQ system using a single 12V DC supply. Fig. 2.2 shows the amplifier circuit used in this thesis. It consists of two stages of CE amplifier stages cascaded one after the other. Voltage-divider configuration is used for biasing to ensure stability in β.

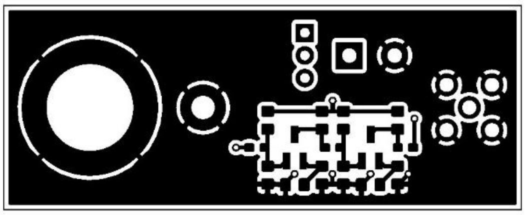

Fig. 2.3 – Pre-amplifier PCB design – top copper layer

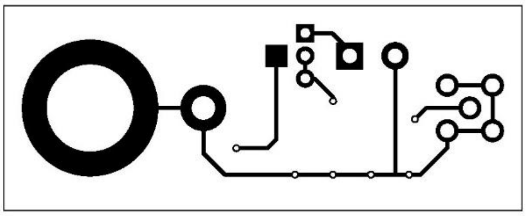

Fig. 2.4 – Pre-amplifier PCB design – bottom copper layer

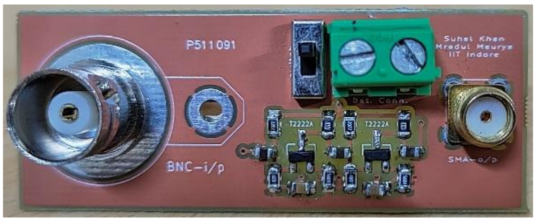

Fig. 2.5 – Pre-amplifier PCB module – top view

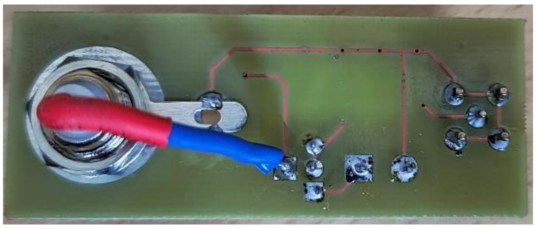

Fig. 2.6 – Pre-amplifier PCB module – bottom view

2.3 Analog to Digital Conversion

This section explains the details of the ADC module developed for the proposed DAQ system. The first subsection discusses how the right ADC was selected for the required application. The next two subsections discuss the two prototype ADC modules developed and tested.

2.3.1 Selection of the ADC

The first and most important part in building the ADC block for any system is to analyse and select the correct ADC for the required application, i.e., acquiring photoacoustic signals. Following are the required specifications of the ADC: -

- Single channel – The PAI system in which the proposed DAQ is supposed to function is single sensor-based. Therefore, an ADC with a single channel is required.
- Parallel output – The digital data from any ADC can be read/transferred either serially or parallelly. Serial transfer implies each digital output bit is read from a single pin one by one. As the resolution of the ADC will increase, the transfer speed of digital data reduces in serial transfer. Parallel output implies all the digital bits would be available on all digital pins at the same time, so that they can be read in a single clock cycle. No matter how high the resolution of the ADC is, all digital bits would be available and can be read in one clock cycle.
- High resolution – Higher resolution means a clearer display of the signal. Since the signal to be read will be in the range of millivolts, a resolution of at least 10 bits is required in order to observe the signal clearly.
- Low analog input range – The amplified signal is specified to be in the range of approximately 600 mV_{PP}. It has to be ensured that the analog input range of the ADC is at least 600 mV_{PP}. On the other hand, a high range would result in increasing of the step size and signal clarity would be lost.
- High sampling rate – It is known that the frequency of the signal is in 3 – 20 MHz range. According to Nyquist criteria, the minimum sampling frequency should be twice the maximum signal frequency. Therefore, the minimum sampling rate of the ADC should be at least 40 MSPS.

In total, four ADC chips were compared in terms of the required specifications. Table 2.1 lists the analysed ADCs and their respective specifications. All four of the listed ADC chips satisfy the criteria of analog input range, frequency and parallel output type. AD9283 was ruled out due to its low resolution. It can be understood that increasing the resolution would result in an increase in power dissipation and cost. Considering both these factors, finally AD9215 was chosen for experimentation. In addition, AD9235 was also considered to be explored in the future if higher resolution was desired.

ADC	Resolution	Analog Input Range	Sampling Rate	Power Dissipation	Output type	Cost
AD9283	8 – bit	1 V_{PP}	Up to 100 MSPS	90 mW	Parallel	Rs. 708
AD9244	14 – bit	1 V_{PP} to 2 V_{PP}	Up to 65 MSPS	550 mW	Parallel	Rs. 4,308
AD9235	12 – bit	1 V_{PP} to 2 V_{PP}	Up to 65 MSPS	300 mW	Parallel	Rs. 1,365
AD9215	10 – bit	1 V_{PP} to 2 V_{PP}	Up to 105 MSPS	120 mW	Parallel	Rs. 1,015

Table 2.1 – Comparison and selection of ADC [36-40]

2.3.2 ADC Module – prototype 1

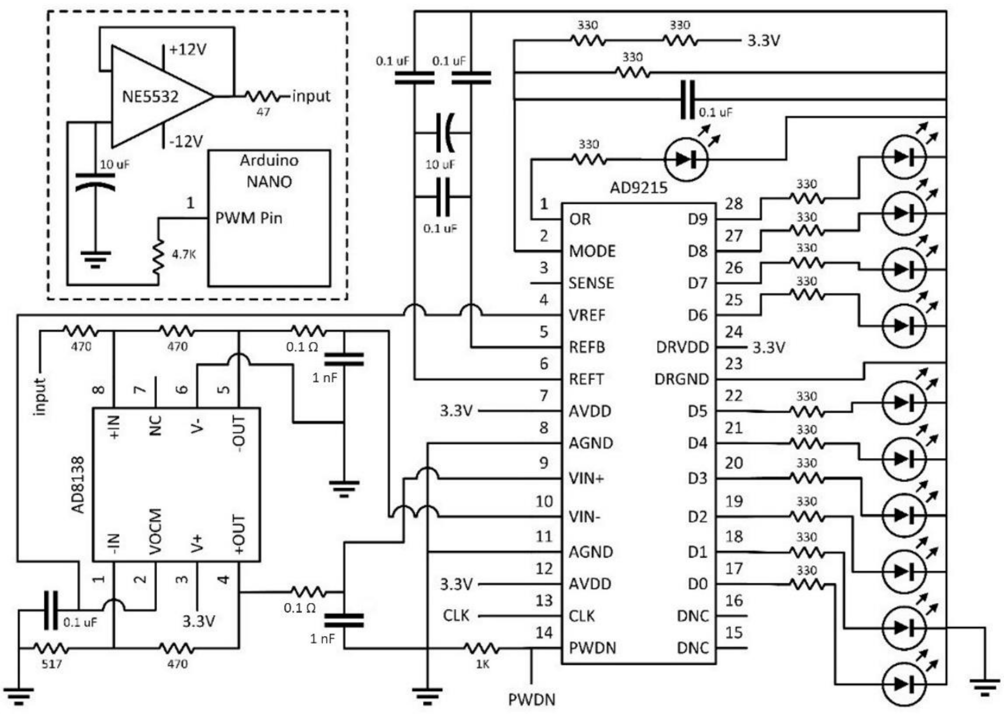

Fig. 2.7 – ADC module – prototype 1 circuit diagram

Fig. 2.7 shows the circuit designed for proper functioning of the selected ADC (AD9215 – 10 bit). AD9215 can be used either in single mode or differential mode, which means the analog input can either be given in single mode or differential mode. Higher SNR can be achieved if input is provided differentially. But the amplifier output is single-ended, therefore a circuit was necessary to convert the signal from single-ended to differential-ended. AD8138, an ADC differential driver IC is used for this application. Its basic function is to convert the input signal into its differential counterparts. The bottom-left part of Fig. 2.7 shows the signal conversion from single-ended to differential-ended. The amplifier output is given to the non-inverting input pin of the differential driver. The inverting input is pulled-down to ground through a resistor. Feedbacks are provided to both inverting and non-inverting inputs. V_{OCM} is the output common mode voltage. The differential outputs will be clamped at a DC voltage equal to V_{OCM}. The two differential outputs are defined by the following formulae: -

$$V_{OUT+} = V_{OCM} + {V_{IN}}/{2}$$

$$V_{OUT-} = V_{OCM} - {V_{IN}}/{2}$$

A DC-clamping voltage is necessary for the differential outputs entering the ADC, because the ADC cannot convert negative voltages (supplied directly). Also, the differential outputs have amplitude half that of input and are out-of-phase with each other. This ensures that when these differential signals are subtracted inside the ADC, the original signal is restored. The subtraction also cancels out the DC-clamping voltage, V_{OCM}. The two differential signals are then passed through low-pass filters to suppress any noise generated in the circuit up until now before entering the ADC.

This small circuit on the top left is a temporary circuit to provide a test input signal. An Arduino NANO is used to first generate an 8 MHz clock for the ADC by using one of the timers. For generating an analog test input signal, a PWM pin was used to generate a triangular wave. Since it is not a true analog signal, it had to be passed through a low pass filter. This signal was then passed through an op-amp configured as a buffer and then a 47 Ω resistance at the output. This was done to make the output impedance of this signal to be 50 **Ω**, which was an essential requirement of the input to AD8138.

The connections done for AD9215 are explained as follows: -

1. Overrange – This pin is 'HIGH' if input exceeds the specified input range (1 V_{PP} or 2 V_{PP}). An output LED is connected on this pin to observe the overrange status.
2. Mode – The different modes of function of AD9215 can be understood from the following table: -

MODE voltage	**Data Format**	**Duty Cycle Stabilizer**
AVDD	Two's complement	Disabled
2/3 AVDD	Two's complement	Enabled
1/3 AVDD	Offset Binary	Enabled
AGND	Offset Binary	Disabled

Table 2.2 – MODE selection [37]

According to the application, the outputs are desired to be in offset binary. Also, AD9215 has an inbuilt duty cycle stabilizer for the input clock, which as the name suggests, keeps the duty cycle of the clock stable at 50%. Therefore, if offset binary data format is to be used and duty cycle stabilizer has to be enabled, MODE voltage should be 1/3 AVDD, so connections in Fig. 2.7 are done accordingly.

3. Sense - The different modes of function of AD9215 can be understood from the following table: -

Selected Mode	**External SENSE connection**	**Resulting V_{REF}**	**Resulting differential span**
Externally supplied reference	AVDD	N/A	2*(External Reference)
Internal 0.5V reference	V_{REF}	0.5 V	1 V_{PP}
Programmed variable reference	External divider	0.5*(1+R2/R1)	2*V_{REF}

Internally programmed 1V reference	AGND	1 V	2 V_{PP}

Table 2.3 – SENSE selection [37]

To get use of the maximum possible input range possible, the ADC is used in the last MODE, 'Internally programmed 1V reference', which provides an input differential span of 2 V_{PP}. Therefore accordingly, SENSE is connected to AGND in Fig. 2.7.

4. V_{REF} – If 'Externally supplied reference' or 'Programmed variable reference' mode is chosen, the external reference must be given as input to this pin. But if internal reference of 0.5V or 1V is used, this pin generates a stable voltage reference of 0.5V or 1V, according to the selection. Since 2 V_{PP} mode is selected, the pin generates a stable 1V reference, which is used as the output common mode voltage for AD8138. It was later observed that using this 1V reference limited the input span of AD8138 to 600mV_{PP}, since it was not mid-supply voltage.
5. REFB – Negative differential reference.
6. REFT – Positive differential reference.

REFB and REFT are defined as: -

$$REFT = {}^{1}/_{2}\,(AVDD + VREF)$$

$$REFB = {}^{1}/_{2}\,(AVDD - VREF)$$

$$Span = 2 * (REFT - REFB) = 2 * VREF$$

REFT and REFB are positive and negative differential voltage reference respectively, and they are responsible for driving the ADC conversion core and establish its input span. Since they are essentially voltage references, decoupling capacitors are connected to these pins for stability.

7. AVDD – This is the analog power supply pin. 3.3 V is given as AVDD.
8. AGND – This is the analog ground pin.
9. V_{IN}+ – This is the in-phase analog input pin. V_{OUT+} from AD8138 is connected to this pin.
10. V_{IN}- – This is the out-of-phase analog input pin. V_{OUT-} from AD8138 is connected to this pin.
11. AGND – This is the analog ground pin.

12. AVDD – This is the analog power supply pin.
13. CLK – This is the clock pin. AD9215 operates on a minimum clock frequency of 5 MHz. A high-speed clock of at least 5 MHz must be provided on this pin. The 'HIGH' and 'LOW' voltages should ideally be 'DRVDD' and 'DGND' with 50% duty cycle. According to these specifications, a clock of 8 MHz generated by Arduino NANO or 5 MHz from the function generator (RIGOL DG1022) was provided.
14. PWDN – This is the power-down pin. This pin when 'HIGH', puts the ADC into sleep-mode to save power. In Fig. 2.7, this pin is pulled down to ground through a resistor since this feature has not been used.
15. DNC – Do not connect pin.
16. DNC – Do not connect pin.
17. D0 – 1st digital output (LSB). An output LED is connected on this pin to observe the bit status.
18. D1 – 2nd digital output. An output LED is connected on this pin to observe the bit status.
19. D2 – 3rd digital output. An output LED is connected on this pin to observe the bit status.
20. D3 – 4th digital output. An output LED is connected on this pin to observe the bit status.
21. D4 – 5th digital output. An output LED is connected on this pin to observe the bit status.
22. D5 – 6th digital output. An output LED is connected on this pin to observe the bit status.
23. DGND – This is the digital ground pin.
24. DRVDD – This is the digital power supply pin. 3.3 V is given as DRVDD.
25. D6 – 7th digital output. An output LED is connected on this pin to observe the bit status.
26. D7 – 8th digital output. An output LED is connected on this pin to observe the bit status.
27. D8 – 9th digital output. An output LED is connected on this pin to observe the bit status.

28. D9 – 10th digital output (MSB). An output LED is connected on this pin to observe the bit status.

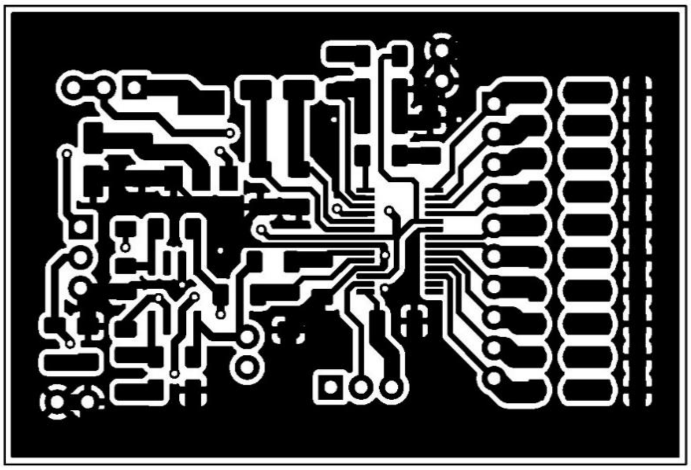

Fig. 2.8 – ADC - prototype 1 PCB design – top copper layer

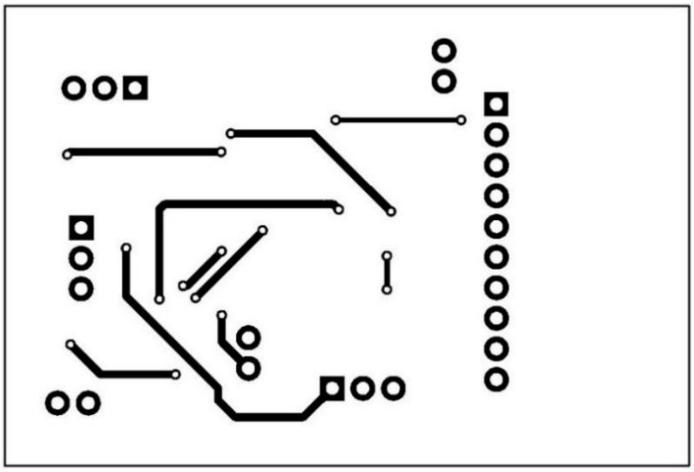

Fig. 2.9 – ADC - prototype 1 PCB design – bottom copper layer

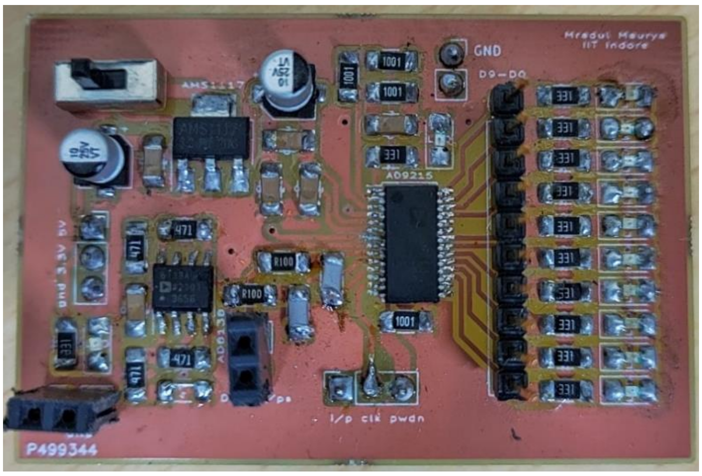

Fig. 2.10 – ADC – prototype 1 PCB module – top view

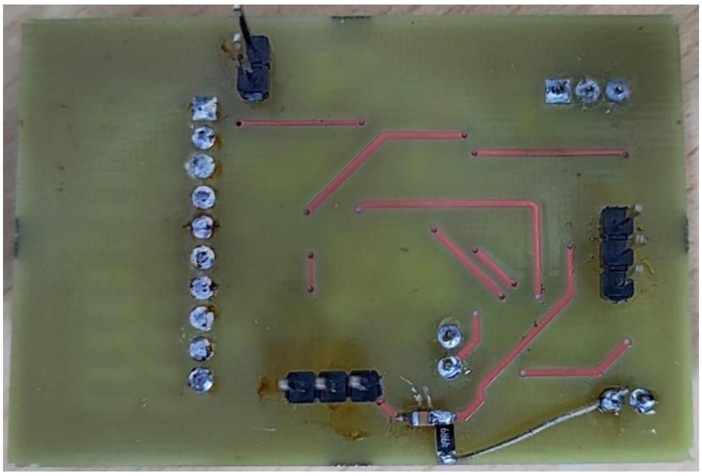

Fig. 2.11 – ADC – prototype 1 PCB module – bottom view

2.3.3 ADC Module – prototype 2

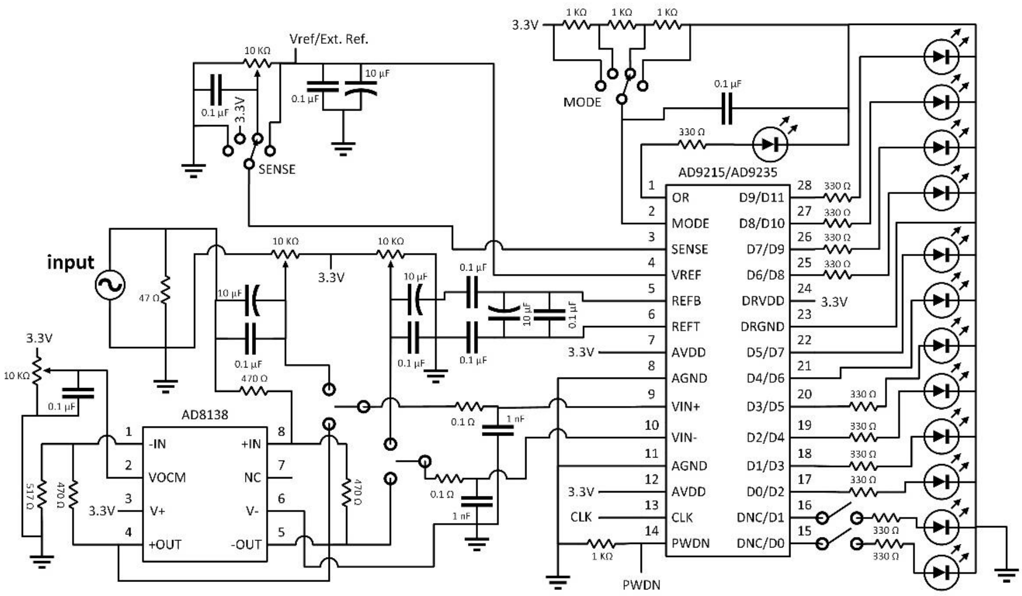

Fig. 2.12 – ADC module – prototype 2 circuit diagram

Fig. 2.12 shows the modified circuit design of the circuit in Fig. 2.7. In this circuit there is an option to either use a 10-bit ADC (AD9215) or a 12-bit ADC (AD9235). The reason why this is possible is because they are both pin-compatible ICs. Pins 1-14 and Pins 23-24 are and serve the same functions. The only differences are that of digital outputs as illustrated in Fig. 2.12. AD9215/AD9235 can be used either in single mode or differential mode, which means the analog input can either be given in single mode or differential mode. Higher SNR can be achieved if input is provided differentially.

To observe the difference in single mode vs differential mode, a single mode circuit has also been included. It can be seen right above the AD8138 IC in Fig. 2.12. In single mode, the positive input (VIN+) receives the original input from the amplifier clamped at some DC voltage and the negative input (VIN-) is clamped at the same DC voltage to cancel the DC voltage on VIN+.

To operate in differential mode, differential signal is needed. But the amplifier output is single-ended, therefore a circuit was necessary to convert the signal from single-ended to differential-ended. AD8138, an ADC differential driver IC is used for this application. Its basic function is to convert the input signal into its differential counterparts. The bottom-left part of Fig. 2.12 shows the signal conversion from single-ended to differential-ended. The amplifier output is given to the non-inverting input pin of the differential driver. The inverting input is pulled-down to ground through a resistor. Feedbacks are provided to both inverting and non-inverting inputs. V_{OCM} is the output common mode voltage. Instead of connecting V_{OCM} to VREF of ADC (as in Fig. 2.7), this time it is made variable by using a potentiometer to experiment and find the ideal voltage values of V_{OCM} to achieve maximum input span. It was observed that mid-supply voltage of 1.65V was the ideal V_{OCM} voltage for maximum voltage range. The differential outputs will be clamped at a DC voltage equal to V_{OCM}. The two differential outputs are defined by the following formulae: -

$$V_{OUT+} = V_{OCM} + {V_{IN}}/{2}$$

$$V_{OUT-} = V_{OCM} - {V_{IN}}/{2}$$

A DC-clamping voltage is necessary for the differential outputs entering the ADC, because the ADC cannot convert negative voltages (supplied directly). Also, the differential outputs have amplitude half that of input and they are out-of-phase with each other. This ensures that when these differential signals are subtracted inside the ADC, the original signal is restored. The subtraction also cancels out the DC-clamping voltage, V_{OCM}. The two differential signals are then passed through low-pass filters to suppress any noise generated in the circuit up until now before entering the ADC.

The amplifier output is given to both single and differential circuits, but two SPDT switches are present to select operation in single mode or differential mode. This ensures only one circuit is operational at a time.

The connections done for AD9215/AD9235 are explained as follows: -

1. Overrange – This pin is 'HIGH' if input exceeds the specified input range (1 V_{PP} or 2 V_{PP}). An output LED is connected on this pin to observe the overrange status.
2. Mode – The different modes of function of AD9215/AD9235 can be understood from the following table: -

MODE voltage	**Data Format**	**Duty Cycle Stabilizer**
AVDD	Two's complement	Disabled
2/3 AVDD	Two's complement	Enabled
1/3 AVDD	Offset Binary	Enabled
AGND	Offset Binary	Disabled

Table 2.2 – MODE selection

Unlike in the circuit of Fig. 2.7, this time, MODE is not fixed. This has been done for experimentation purposes. Connections for all four modes are done, and a 4-way switch is present to select between them.

3. Sense - The different modes of function of AD9215 can be understood from the following table: -

Selected Mode	**External SENSE connection**	**Resulting V_{REF}**	**Resulting differential span**
Externally supplied reference	AVDD	N/A	2*(External Reference)
Internal 0.5V reference	V_{REF}	0.5 V	1 V_{PP}
Programmed variable reference	External divider	0.5*(1+R2/R1)	2*V_{REF}

Internally programmed 1V reference	AGND	1 V	2 V_{PP}

Table 2.3 – SENSE selection

Unlike in the circuit of Fig. 2.7, this time, SENSE is not fixed. This has been done for experimentation purposes. Connections for all four sense connections are done, and a 4-way switch is present to select between them.

4. V_{REF} – If 'Externally supplied reference' or 'Programmed variable reference' mode is chosen, the external reference must be given as input to this pin. But if internal reference of 0.5V or 1V is used, this pin generates a stable voltage reference of 0.5V or 1V, according to the selection.
5. REFB – Negative differential reference.
6. REFT – Positive differential reference.

REFB and REFT are defined as: -

$$REFT = {}^{1}/_{2}\,(AVDD + VREF)$$

$$REFB = {}^{1}/_{2}\,(AVDD - VREF)$$

$$Span = 2 * (REFT - REFB) = 2 * VREF$$

REFT and REFB are positive and negative differential voltage reference respectively, and they are responsible for driving the ADC conversion core and establish its input span. Since they are essentially voltage references, decoupling capacitors are connected to these pins for stability.

7. AVDD – This is the analog power supply pin. 3.3 V is given as AVDD.
8. AGND – This is the analog ground pin.
9. V_{IN}+ – This is the in-phase analog input pin. V_{OUT+} from AD8138 is connected to this pin.
10. V_{IN}- – This is the out-of-phase analog input pin. V_{OUT-} from AD8138 is connected to this pin.
11. AGND – This is the analog ground pin.
12. AVDD – This is the analog power supply pin.
13. CLK – This is the clock pin. AD9215/AD9235 operates on a minimum clock frequency of 5 MHz. A high-speed clock of at least 5 MHz must be provided on this pin. The 'HIGH' and 'LOW' voltages should ideally

be ‘DRVDD’ and ‘DGND’ with 50% duty cycle. According to these specifications, a clock of 5 MHz is provided from the function generator (RIGOL DG1022).

14. PWDN – This is the power-down pin. This pin when ‘HIGH’, puts the ADC into sleep-mode to save power. In Fig. 2.12, this pin is pulled down to ground through a resistor since this feature has not been used.
15. DNC/D0 – Do not connect pin (AD9215) or 1st digital output (LSB) (AD9235). An output LED via a switch is connected on this pin to observe the bit status. This switch is open when AD9215 is used and is closed when AD9235 is used.
16. DNC/D1 – Do not connect pin (AD9215) or 2nd digital output (AD9235). An output LED via a switch is connected on this pin to observe the bit status. This switch is open when AD9215 is used and is closed when AD9235 is used.
17. D0/D2 – 1st digital output (LSB) (AD9215) or 3rd digital output (AD9235). An output LED is connected on this pin to observe the bit status.
18. D1/D3 – 2nd digital output (AD9215) or 4th digital output (AD9235). An output LED is connected on this pin to observe the bit status.
19. D2/D4 – 3rd digital output (AD9215) or 5th digital output (AD9235). An output LED is connected on this pin to observe the bit status.
20. D3/D5 – 4th digital output (AD9215) or 6th digital output (AD9235). An output LED is connected on this pin to observe the bit status.
21. D4/D6 – 5th digital output (AD9215) or 7th digital output (AD9235). An output LED is connected on this pin to observe the bit status.
22. D5/D7 – 6th digital output (AD9215) or 8th digital output (AD9235). An output LED is connected on this pin to observe the bit status.
23. DGND – This is the digital ground pin.
24. DRVDD – This is the digital power supply pin. 3.3 V is given as DRVDD.
25. D6/D8 – 7th digital output (AD9215) or 9th digital output (AD9235). An output LED is connected on this pin to observe the bit status.
26. D7/D9 – 8th digital output (AD9215) or 10th digital output (AD9235). An output LED is connected on this pin to observe the bit status.

27. D8/D10 – 9th digital output (AD9215) or 11th digital output (AD9235). An output LED is connected on this pin to observe the bit status.
28. D9/D11 – 10th digital output (MSB) (AD9215) or 12th digital output (MSB) (AD9235). An output LED is connected on this pin to observe the bit status.

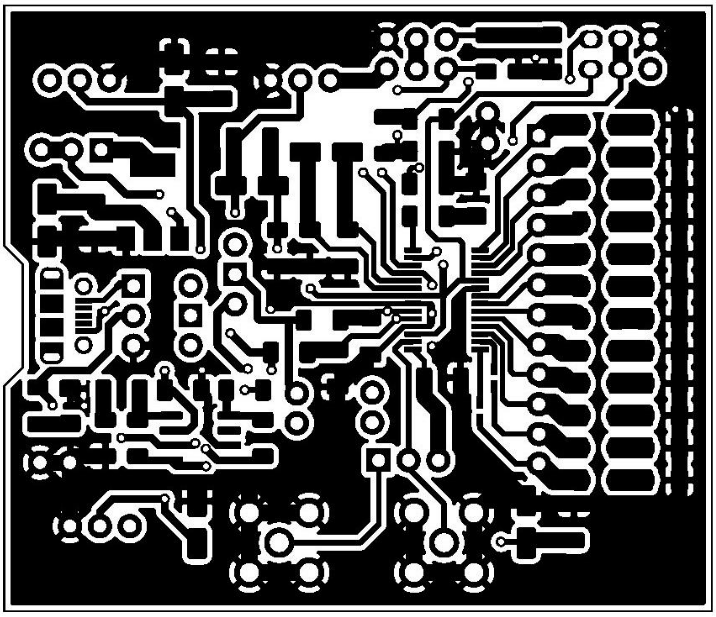

Fig. 2.13 – ADC – prototype 2 PCB design – top copper layer

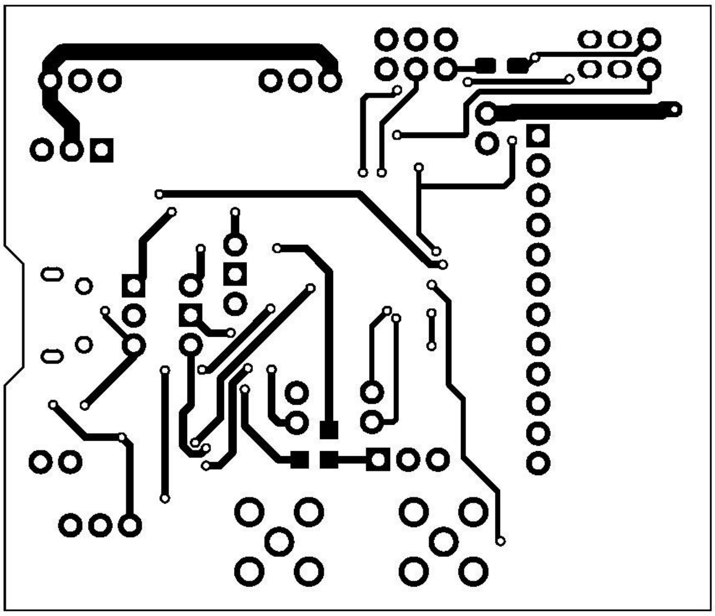

Fig. 2.14 – ADC – prototype 2 PCB design – bottom copper layer

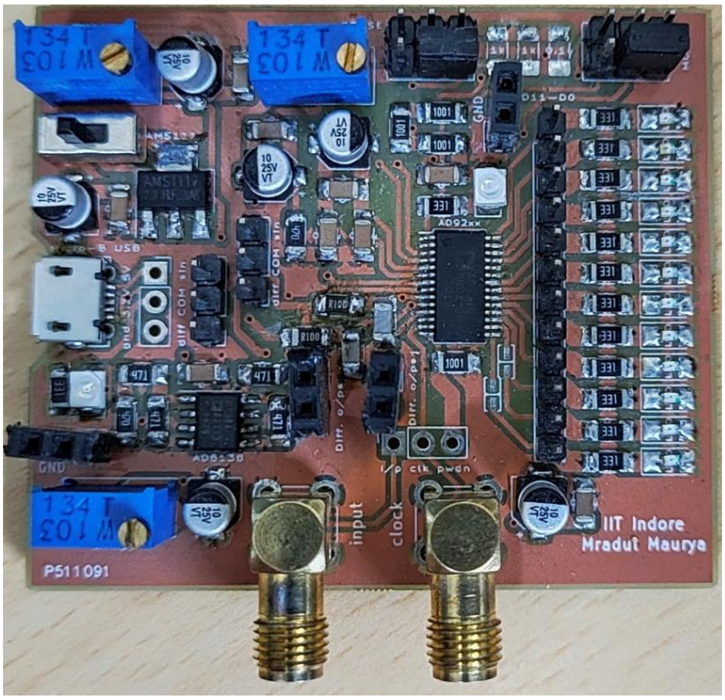

Fig. 2.15 – ADC – prototype 2 PCB module – top view

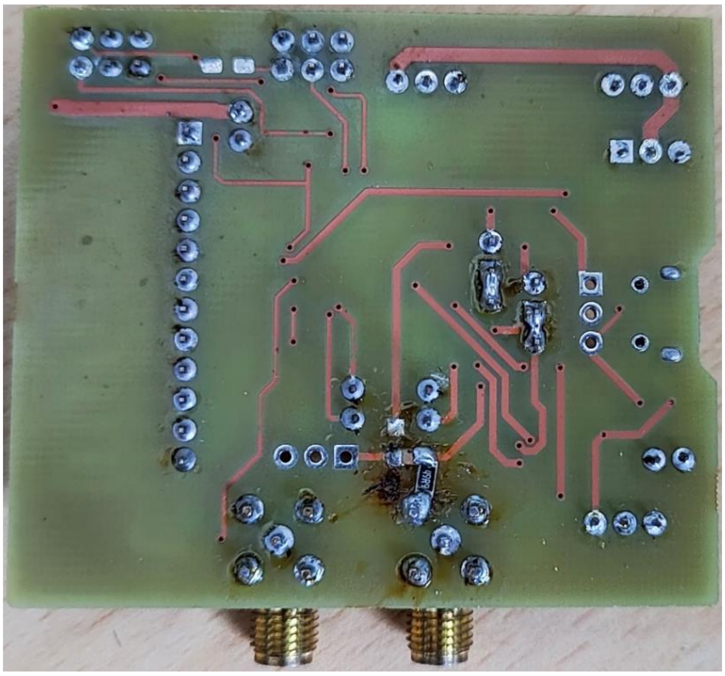

Fig. 2.16 – ADC – prototype 2 PCB module – bottom view

2.4 Building the System

Building the ADC module was one of the most important tasks in building the proposed DAQ. Following that, other minor challenges were addressed, and after that, putting together all the blocks to build the proposed DAQ system. The first subsection discusses the microcontroller used for acquiring, storing and sending data. The next three subsections discuss the use of this microcontroller to generate a high frequency clock and then developing PCB modules to purify it before giving it to the ADC. The final sections discuss the DAQ built after assembling all the blocks developed.

2.4.1 STM32F446RE microcontroller board

It has been discussed in the above sections that photoacoustic signals lie in the 3 to 20 MHz spectrum, and that is why an ADC having a sampling rate of at least 40 MSPS was needed and chosen. This data from the ADC has to be read and stored somewhere. In the proposed DAQ system, a high-speed microcontroller has been used for that purpose. The most important parameter that needs to be kept in mind is that the GPIOs reading the digital data coming from the ADC, should be able to keep up with the high conversion and transfer rate of the ADC. In technical terms, that would mean the toggle rate of the GPIOs must be at least 40 MSPS. The microcontroller must also be able to generate a high-frequency clock for the ADC using a timer and also have an inbuilt hardware interrupt so that the external trigger coming from the LASER setup can be also be incorporated. All this would be discussed in detail in the following sections.

According to the needs discussed above, NUCLEO-64 – STM32F446RE microcontroller board was finally chosen to be used for our application. Following are the useful specifications of the board [28]: -

- ARM 32-bit Cortex-M4 CPU
- Clock frequency up to 180 MHz
- 512 KB of flash memory, 128 KB of SRAM
- Up to 17 timers: two watchdog timers, one SysTick timer, twelve 16-bit timers and two 32-bit timers up to 180 MHz
- Three 16-bit GPIO ports, i.e., a total of 48 general purpose I/Os. Each pin can be programmed as an interrupt and can toggle at a rate up to 90 MHz

- Up to 20 communication interfaces including but not limited to, SPI, I^2C, USART and UART

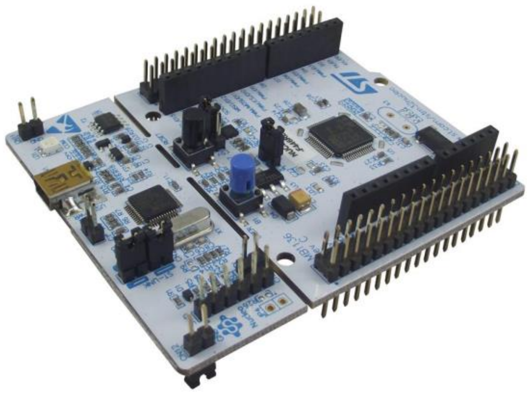

Fig. 2.17 – NUCLEO – F446RE microcontroller development board [29]

2.4.2 Clock generation

In all the experiments conducted on the ADC prototype PCBs, for the purpose of providing the clock for the ADC, a function generator (RIGOL DG1022) has been used. But in a real-time DAQ system, using a function generator would be tedious and highly impractical. Therefore, in order to get rid of the function generator, an alternative solution is proposed. For storing and acquiring the digital data coming from the ADC, a microcontroller will be used. A microcontroller contains several peripherals of its own, including something of interest, i.e., timers. Using one of the many timers present in STM32F446RE microcontroller, it is possible to generate a very high-speed clock. STM32F446RE microcontroller board runs on a clock frequency of 180 MHz. The theoretical maximum frequency of a clock that can be generated through one of its timers is 90 MHz and the desired frequency can be achieved by varying the 3 parameters, namely, Prescaler, period and pulse. The frequency and duty cycle of the clock can be adjusted using the following formulae: -

$$Frequency = \frac{180}{Period * (Prescaler + 1)}$$

$$Duty\ Cycle = \frac{Pulse}{Period} * 100$$

Generating a high-speed clock is theoretically possible according to the STM32F446RE datasheet. But it was observed that at higher frequencies (> 5

MHz), distortion increases, spikes are observed on rising and falling edges and at even higher frequencies, amplitude degradation is observed. Therefore, there is a need for purification of this ‘raw’ clock generated from the microcontroller, before it reaches the ADC. The upcoming sections discuss the proposed prototype circuits for purification of the clock.

2.4.3 Clock purification circuit – prototype 1

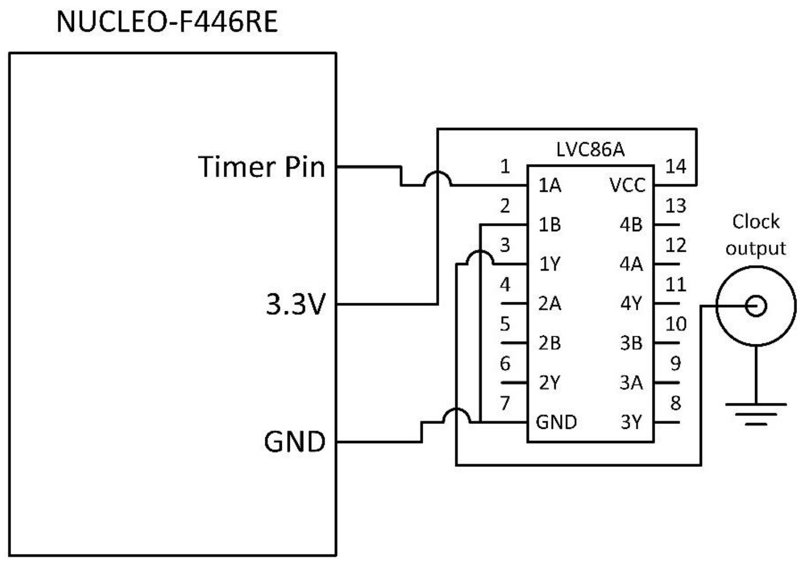

Fig. 2.18 – CPC-P1 circuit diagram

The ADC being used to convert analog data to digital data requires a high-speed clock to function. The microcontroller that is being used to capture and store the digital data, NUCLEO-F446RE, is also being used to generate the required clock for the ADC. But at high frequencies (>5 MHz), overshoots, undershoots and amplitude degradation is observed in the clock generated by the microcontroller’s timer. Therefore, there is a need for a clock purification circuit after the microcontroller before it reaches the ADC. Fig. 2.18 shows the first experimental design for the required need. LVC86A is a XOR-gate IC. By property of a XOR-gate, if one input is ‘0’, output is the same as the other input. In other words, it acts like a buffer. In Fig. 2.18, it can be observed that one input of XOR-gate is the timer-generated clock from the microcontroller, the second input is grounded and the output is observed.

There were a few shortcomings to this design: -

- The observed toggle rate of the IC was limited to approximately 15 MHz only.
- Amplitude degradation was observed at frequencies exceeding 15 MHz. Since switching threshold is fixed, amplitude degraded at higher frequencies cannot be restored.
- Rise and fall times are relatively high. Therefore, sharp clock edges were not observed.
- The amplitude of overshoots/undershoots increases after passing through this circuit.

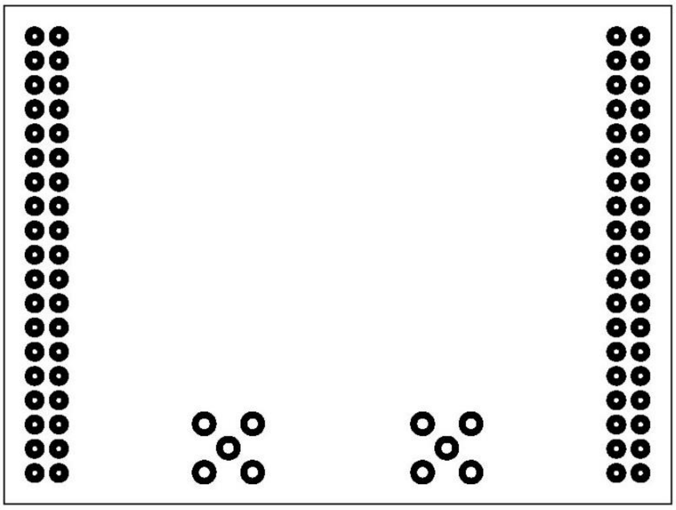

Fig. 2.19 – CPC-P1 PCB design – top copper layer

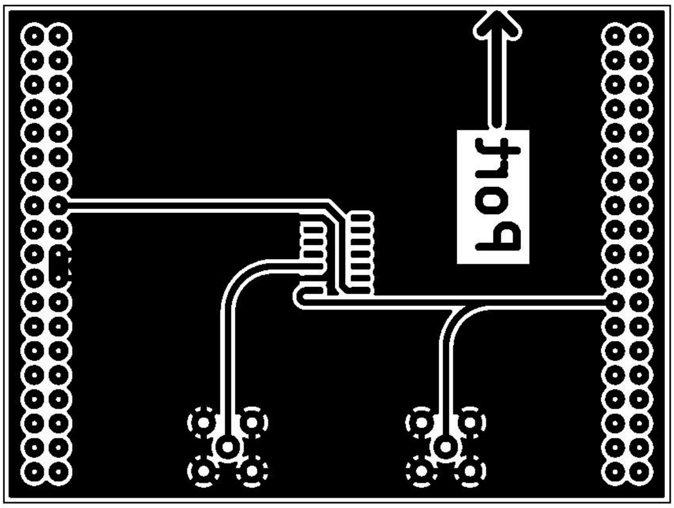

Fig. 2.20 – CPC-P1 PCB design – bottom copper layer

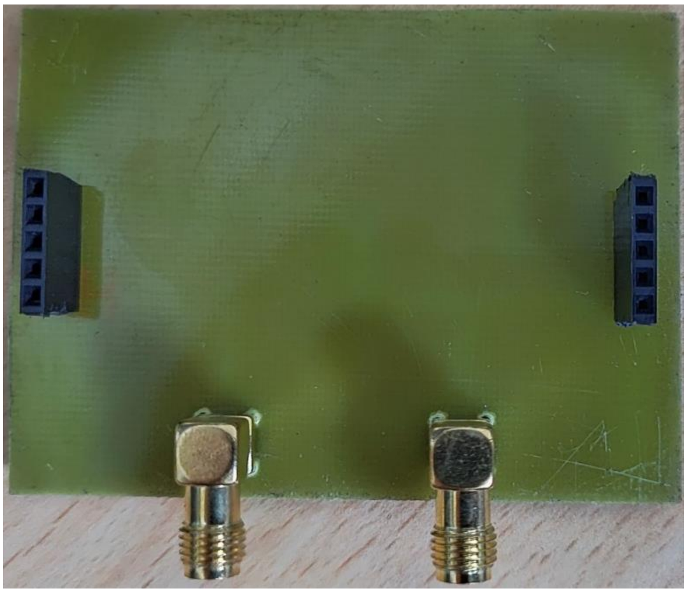

Fig. 2.21 – CPC-P1 PCB module – top view

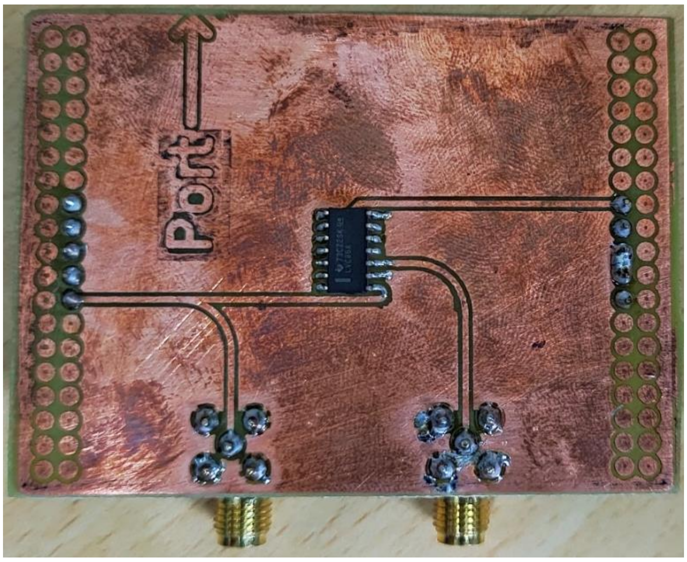

Fig. 2.22 – CPC-P1 PCB module – bottom view

2.4.4 Clock purification circuit – prototype 2

Fig. 2.23 shows the second experimental approach to purify the timer-generated clock from the microcontroller. In this circuit, a very-high-speed comparator is used. Using this approach, all four issues from the XOR-gate approach were solved. Since the maximum toggle rate of this comparator is 80 MHz, high-speed switching can be achieved. Since threshold can be adjusted, degradation in amplitude can also be compensated and rise and fall times are also very low which result in sharp clock edges. TLV3501 is the comparator that has been used for the application. The clock is given as input to the non-inverting input pin of the comparator. On the inverting input pin, the variable threshold is given. On V+ and V- pins, the 'logic-HIGH' voltage and 'logic-LOW' voltages are connected, which are 3.3V and 0V respectively. SHDN pin is the shutdown pin of the IC. If this pin is 'HIGH', the device goes into sleep mode. If this pin is 'LOW', the device is active. That is why in the circuit, it is connected to V-, since we are not making use of the shutdown feature of this IC.

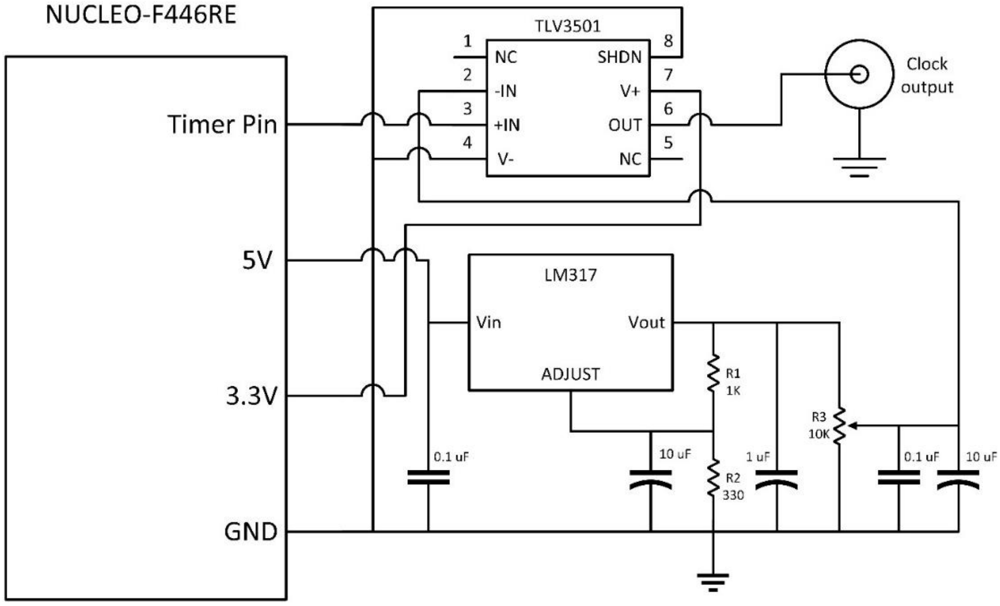

Fig. 2.23 – CPC-P2 circuit diagram

To generate the variable threshold, a separate circuit has been used. 0 – 1.68V variable voltage has been created using LM317, which is a 1.25V – 37V variable voltage regulator IC. The output voltage of LM317 can be controlled using the following formula: -

$$V_{OUT} = V_{REF} * \left(1 + {}^{R2}/_{R1}\right) + (I_{ADJ} * R2)$$

According to the datasheet of LM317, V_{REF} = 1.25V and I_{ADJ} = 50uA. Since 'HIGH' and 'LOW' voltage of the required clock are 3.3V and 0V, the maximum threshold required would be mid-voltage, i.e., 1.65V. For ease in calculation, (I_{ADJ}*R2) part is neglected. So, putting the V_{OUT} and V_{REF} values, (R2/R1) comes out be 0.32. If R1 is chosen to be 1 KΩ, R2 would be 320 Ω. The closest standard resistor value is 330 Ω, so that was chosen. Putting these two resistor values in the equations yields an output voltage of 1.68V. Now this voltage is given to a 10 KΩ precision trimmer, giving a variable threshold of 0 to 1.68V. The capacitors seen in the LM317 circuit are placed for voltage stability.

The only shortcoming to this circuit was that the variable threshold generated using the trimmer was unstable at thresholds less than 1 V. This issue is solved by incorporating a new variable threshold circuit which uses LT3080, which is a precision low-voltage reference IC. The details of the same will be discussed in following section.

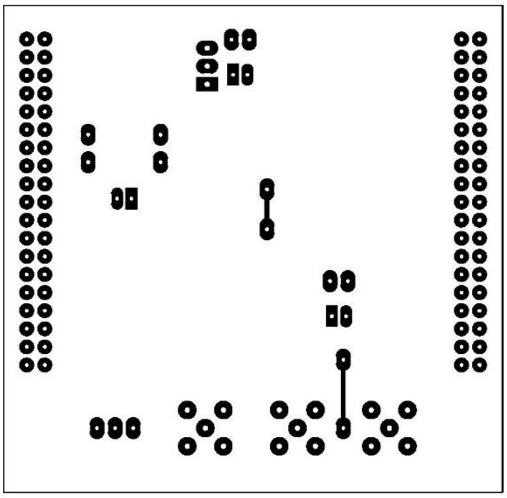

Fig. 2.24 – CPC-P2 PCB design – top copper layer

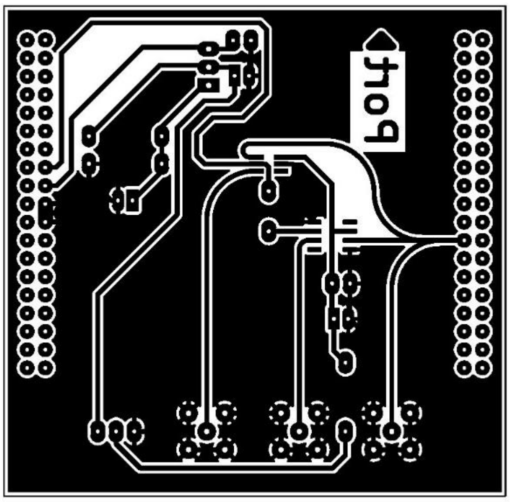

Fig. 2.25 – CPC-P2 PCB design – bottom copper layer

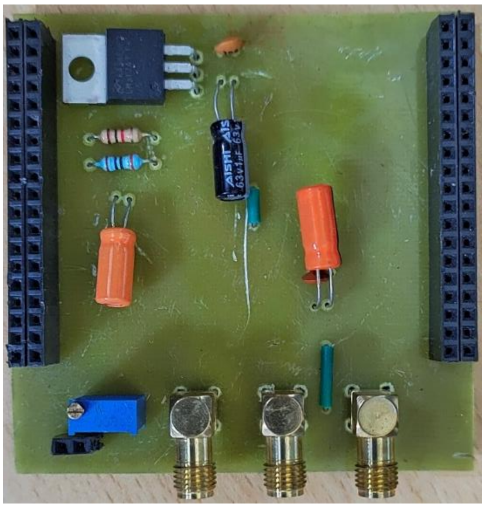

Fig. 2.26 – CPC-P2 PCB module – top view

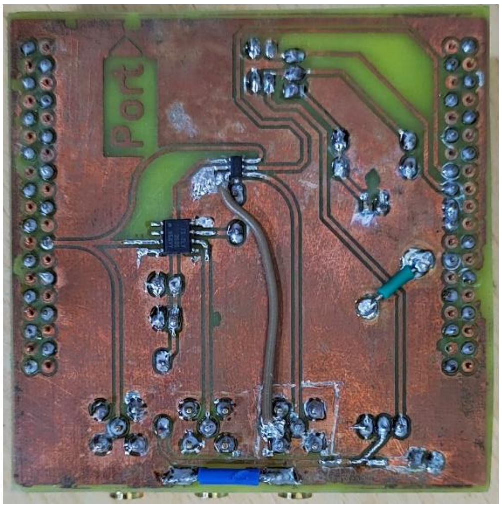

Fig. 2.27 – CPC-P2 PCB module – bottom view

2.4.5 DAQ – prototype 1

Fig. 2.28 shows the first prototype circuit of the DAQ designed and developed. The circuit on the right is the clock generation and purification circuit. Using the same concept of a comparator (Fig. 2.23), the circuit has been made. The only change is using LT3080, a high-precision voltage reference IC, instead of LM317. The output voltage can be varied by means of a single resistor. Following is the formula: -

$$V_{OUT} = 10uA * R_{SET}$$

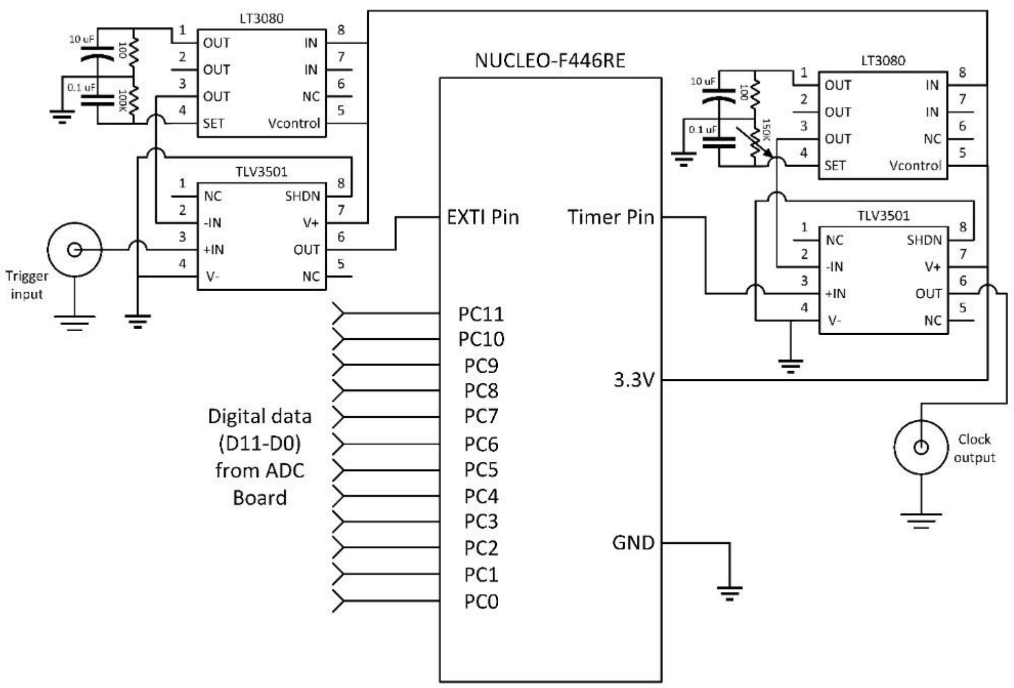

Fig. 2.28 – DAQ – prototype 1 circuit diagram

LT3080 has a high-precision current source of 10uA which flows out from the 'SET' pin. So, depending upon the resistor value connected at the 'SET' pin, output voltage can be adjusted accordingly using the above formula. If 1.65V is desired, R_{SET} would be 165K. The closest standard resistor value is 150K, therefore, it was chosen. Using this IC solved the voltage reference stability issue faced in the last circuit (Fig. 2.23).

For synchronous signal-acquisition for averaging, a trigger signal is given to the microcontroller as input to one of its interrupts. The problem is that the 'HIGH' voltage of the trigger signal is approximately 1.5V. The microcontroller being used is 3.3V-based. So, a threshold of 1.65V defines a signal level 'HIGH' or 'LOW'. Since the trigger voltage does not exceed 1.5V, rising edges/levels won't be recognised by the microcontroller. Therefore, there was a need to boost the amplitude of the trigger signal before it reaches the microcontroller. The same comparator approach has been used for it. The circuit on the left is exactly same as the circuit on the right. By setting R_{SET} to be 100 KΩ, a threshold of 1V is ensured, and the new 'HIGH' and 'LOW' levels would be 3.3V and 0V respectively.

The microcontroller has also been used to capture and store the digitally-converted signal, the 10/12-bit output from the ADC has been connected to

10/12 GPIO pins of PORTC. If AD9215 (10-bit) is used, PC9 to PC0 are used. If AD9235 (12-bit) is used, PC11 to PC0 are used.

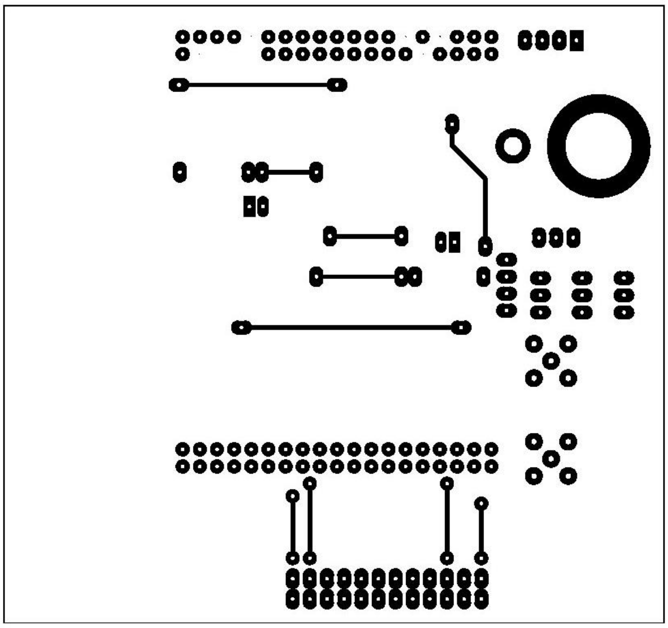

Fig. 2.29 – DAQ prototype 1 PCB design – top copper layer

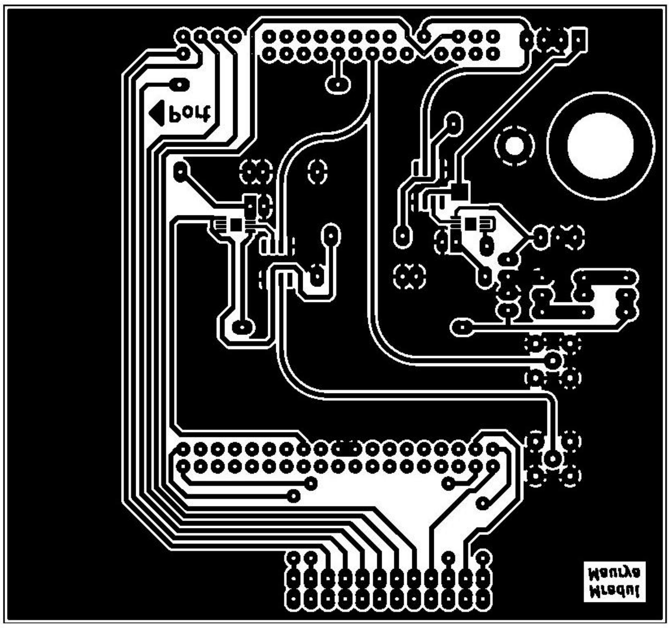

Fig. 2.30 – DAQ prototype 1 PCB design – bottom copper layer

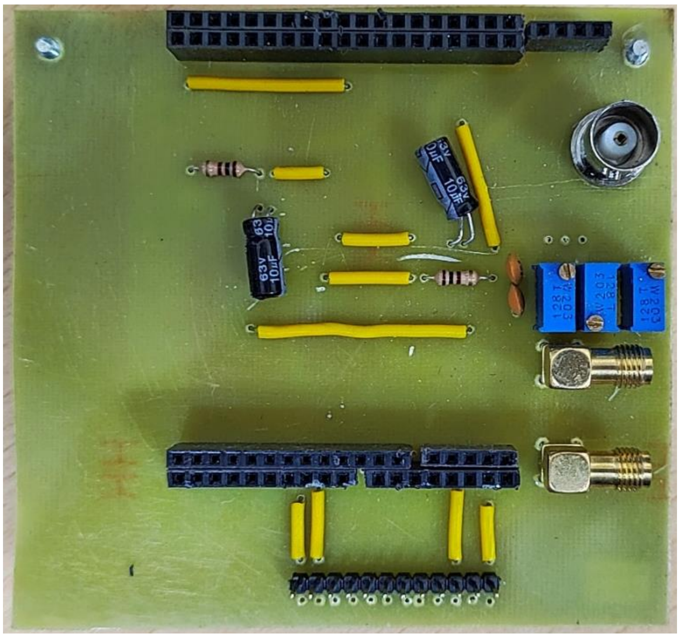

Fig. 2.31 – DAQ prototype 1 PCB module – top view

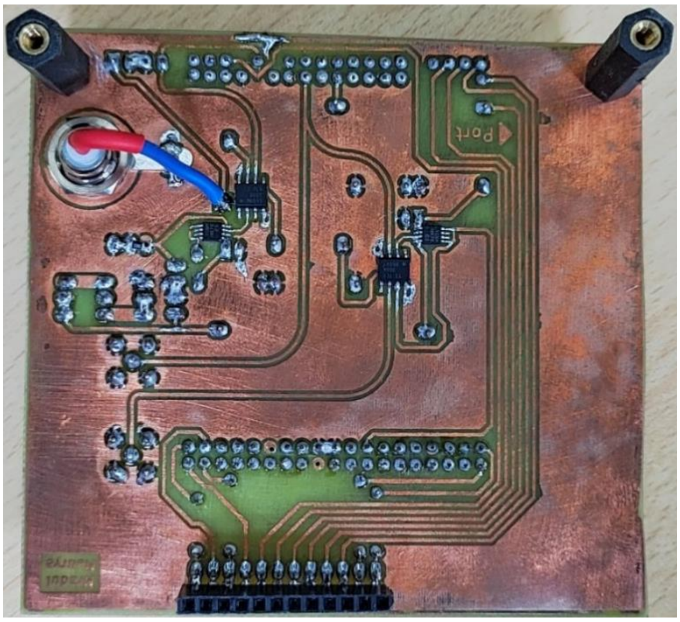

Fig. 2.32 – DAQ prototype 1 PCB module – bottom view

2.4.6 DAQ – prototype 2

In the previous sections, separate components of the DAQ were designed and tested. To increase the system's compactness even further, all those components were designed into a single PCB. Designing the PCB proved to be quite challenging. One thing that was observed during the experiments on previous prototypes of ADCs was that the input signal becomes too noisy when clock is switched ON. The reason for this is because in previous versions of PCB, the high-frequency clock and input traces were running very close and parallelly, resulting in super-imposing of clock over the input signal. This problem is solved in the new design by keeping the clock and input traces far away from each other.

In advanced PCB designing, it is a good practice to use a ground plane. This greatly reduces EMI and prevents generation of internal noise from components and copper traces. Each bend in a copper trace contributes to some amount of noise and the noise increases if the signal running through it is of high frequency. Although it is almost impossible to have none of the traces without any bends, but it is possible to reduce the number of bends by careful and intelligent PCB routing. A very important point which is many times overlooked is that current does not just vanish abruptly as soon as it reaches the ground connection. The current still must go back to its source (i.e., power supply). So, if the return current faces too many bends in its copper trace path, it would result in generation of internal noise. This is the reason, in a good PCB design, it is suggested to use one layer to place components and route traces and dedicate an entire layer to ground. In the proposed PCB design, to route a connection to ground, a small trace in run on the routing layer and then connected to the ground plane through a via. Since the ground plane has a very small area occupied by traces (short jumpers to assist in routing as it is practically impossible to route on a single layer), the return current now has path to the source with minimum to no bends, which results in great reduction of internal noise.

In a circuit containing an ADC, both analog and digital signals have to dealt with. These systems are called mixed-signal systems. These systems are highly susceptible to noise and interference and thus are difficult to handle. The pin configuration of almost all ADCs has two supplies, AVDD and DVDD/DRVDD and two grounds AGND and DGND/DRGND. These terms are used to differentiate between analog supply (AVDD), digital supply (DVDD/DRVDD), analog ground (AGND), and digital ground (DGND/DRGND). Separate supplies for analog and digital circuitry are needed because digital signals are sharp-transitioned and have a high frequency, whereas the frequency of analog signals is generally low as compared to digital signals and they are also slow transitioned. These two differences are enough for analog and digital signals to interfere with each other. To reduce this interference, the supplies and grounds of analog and digital circuits are separated. This also applies to DC signals (which are ideally zero-frequency signals). If a high-frequency digital trace runs close to, above or below a DC or analog trace, the stability of it is sure to be disturbed. So, keeping this in mind, no analog or DC trace is run close to or above or below a digital trace in the new PCB design.

Separating analog and digital circuits greatly reduces high-frequency noise. But it should not be forgotten that in a system, there can only be one single ground ('star' topology). So, the analog and digital ground planes are connected at one single point, which is then routed to the ground of the main power supply.

While transmitting digital signals, there should ideally be zero bends in the copper trace carrying this signal. But it is practically impossible to achieve that. Having bends results in few problems, including overshoots/undershoots in rising/falling edges. Making an acute-angle bend results in more overshoot than an obtuse-angle bend. So, as the angle of bend increases, overshoot/undershoot reduces. Utilizing this concept, in the new PCB design, the curved-trace method has been incorporated to transport the high-speed clock from the microcontroller (where it is generated) to the ADC. A curved trace is essentially many small and straight traces connected at large obtuse angles. This approach almost completely eliminates overshoots/undershoots in the high-speed clock signal.

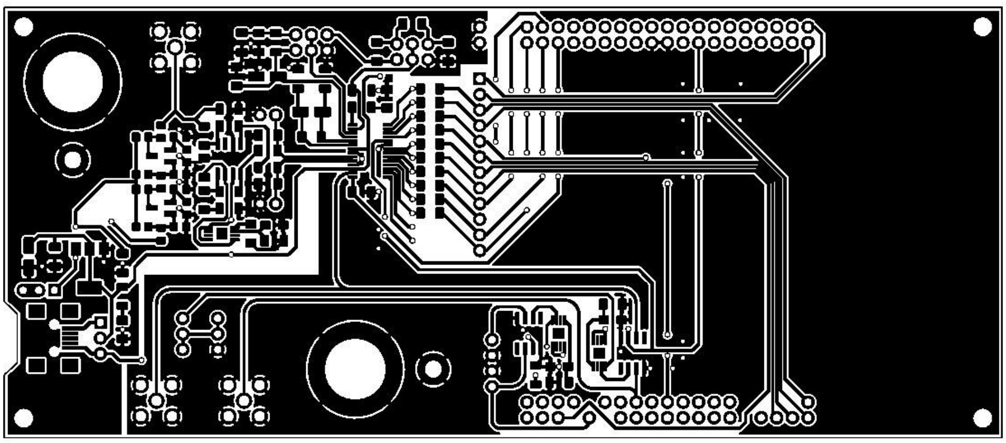

Fig. 2.33 – DAQ prototype 2 PCB design – top copper layer

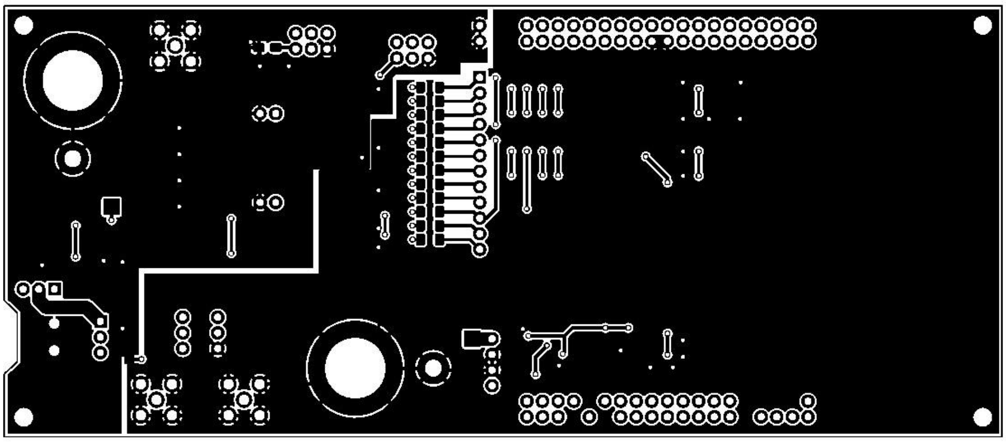

Fig. 2.34 – DAQ prototype 2 PCB design – bottom copper layer

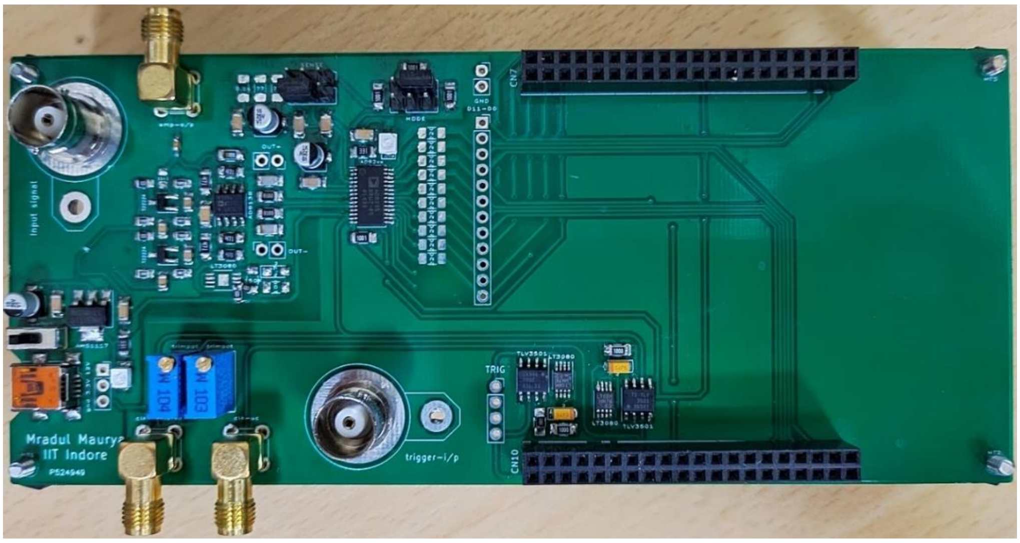

Fig. 2.35 – DAQ prototype 2 PCB module – top view

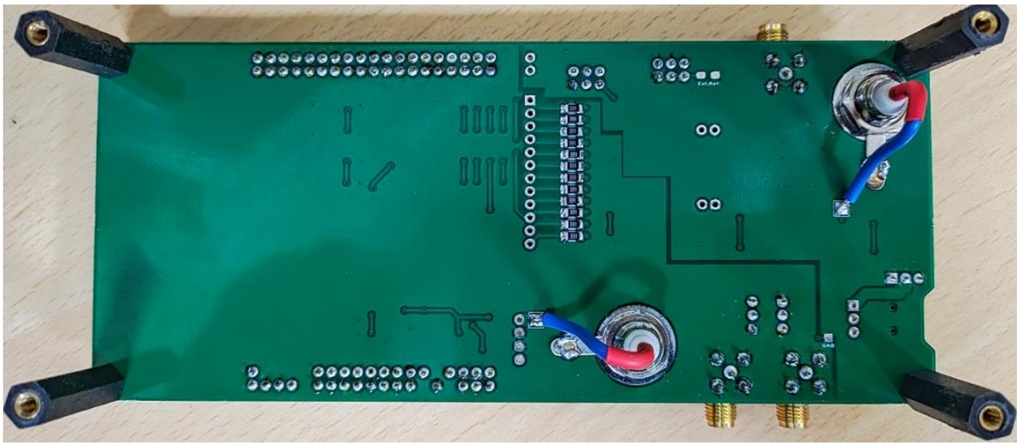

Fig. 2.36 – DAQ prototype 2 PCB module – bottom view

This DAQ consists of all the components of the proposed system, namely pre-amplifier, ADC, clock generation and purification, trigger signal restoration, acquisition of data in microcontroller and sending it to the PC. The design is made such that separate blocks can be tested individually. All the blocks were tested and they replicated the known results from their previous prototype PCB, except the ADC differential driver circuit. It was observed that an arbitrary noise is being generated from the PCB, which is superimposing on all DC as well as analog signals. The root cause of this issue could not be found, despite several attempts of debugging. Therefore, this aspect might be explored in the future. If the proposed DAQ prototype can successfully be debugged, it might result in accurate and noise-free acquisition of photoacoustic signals.

2.5 Signal Acquisition

2.5.1 Microcontroller algorithm for data acquisition

Note: - In this section, AD9235 (12-bit ADC) has been used in all ADC references.

Fig. 2.37 shows the flow of the microcontroller code to read the digital data from the ADC, process it and send it to PC. Before commencing operation, the microcontroller initializes all the variables and peripherals, including the GPIOs, the trigger interrupt and the clock-generating timer. It is stated in the above sections that the photoacoustic signal to be acquired has a very low SNR. To eliminate the noise, or increase the SNR of the signal, signal averaging technique is being used. The signal is acquired multiple times and then averaged to produce the final signal. Greater the number of times averaging is done, greater will be the SNR. The signal is being acquired 4000 times to be averaged later. The first condition check will be if the signal has been acquired 4000 times or not. If not, the second condition check will be if the trigger signal has interrupted the microcontroller or not. The trigger signal plays an important role in multiple acquisition and averaging. For preventing the loss of signal during averaging, it is to be ensured that the signal acquisition is done at a predefined constant interval, so that the actual signal comes at the same time frame in all acquisitions. After the trigger signal interrupts the microcontroller, acquisition starts. A total of 2500 samples of the signal are being acquired. The sampling interval of the microcontroller is around 55 ns. That amounts to approximately 140 µs of the signal being captured in each acquisition.

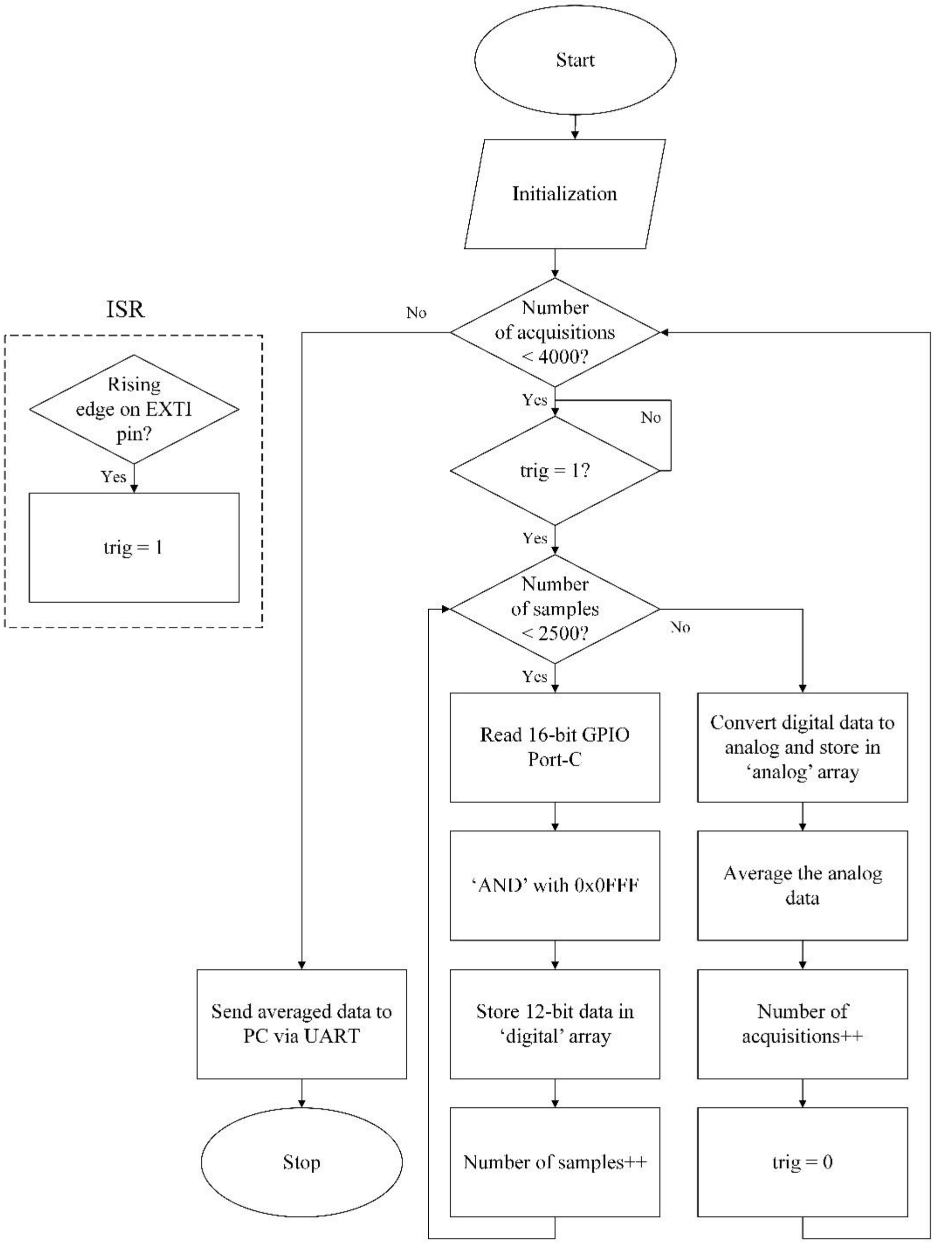

Fig. 2.37 – Flow of the microcontroller code

The STM32F446RE microcontroller provides GPIOs as 16 – bit ports. The ADC that is being used provides the digital output in a 12-bit format. And since we need to read the digital data parallelly, we cannot serially read each of the 12 GPIOs. In the microcontroller code, *'GPIO –> IDR'* command is being utilised for parallel reading. IDR stands for Input Data Register. It is being used as follows: -

```
uint16_t data_digital[samples];

…

for (i = 0; i < samples; i++)

{

	data_digital[i] = GPIOC->IDR & 0x0FFF;

}

…
```

data_digital is an array in which each value is a 16 – bit unsigned integer. Inside the '*for*' loop, three operations are being performed. *GPIO –> IDR* gives the logic state of all GPIO pins in PORT C as a 16 – bit binary number. After that, logical *'AND'* operation is being performed between this 16 – bit number and another hexadecimal number *0x0FFF*, which is *0000 1111 1111 1111* in binary. This number is essentially the last 12 bits '1' and the rest '0'. By performing *'AND'* operation with *0x0FFF*, it is ensured that only the states of the 12 GPIOs that are connected to the 12-bit digital output of the ADC are considered and the rest floating pins are discarded. After this operation, this 16 – bit number is converted into its equivalent integer value, because it has to be stored in the 16 – bit unsigned integer array, *data_digital*.

When all 2500 samples of a single acquisition have been acquired, this data is converted into analog data by using the following formula: -

$$d_a(mV) = 1000.00 * \left(\frac{a_{max} - a_{min}}{2^n - 1} * d_d + a_{min}\right)$$

where, n *= resolution of the ADC*

d_a *= equivalent analog value of digital data*

d_d *= decimal equivalent of n – bit digital data*

a_{max} *= upper limit of the ADC's analog input range*

a_{min} *= lower limit of the ADC's analog input range*

After this digital to analog conversion, averaging of the signal is done. There can be two approaches. First is to collect and store all the signal acquisitions and then take the average. But this method requires a lot of memory and is thus, impractical. The method used in this thesis is memory-efficient. The following formula is used: -

$$d_{a,avg}(mV) = \frac{\left(d_{a,avg} * i + d_a\right)}{i+1}$$

This formula keeps overwriting the same array after taking average of all the signals till i^{th} acquisition.

The above process completes one single acquisition. This process has to be repeated 4000 times for averaging the signal 4000 times. But before that, the 'trig' variable has to be set to 0. It is to be noted that this variable is programmed to be set when the external trigger signal arrives on the interrupt. After calculation of the final averaged signal, this is sent via UART communication to the PC, where the signal values are stored in a csv file for further analysis and display.

2.5.2 Calculation of sampling interval

The sampling interval decides the amount of signal captured by a fixed number of samples. In the microcontroller code snippet shown in the Section 2.5.1, it may be observed that no delay has been introduced after a single sample capture. This means that the microcontroller is at its limit and we cannot further speed up the acquisition process since the time gap between any two samples is the time in which the essential instructions like reading, copying, storing, incrementing, etc. are being executed. That time gap, or the sampling interval has been measured by using the following method: -

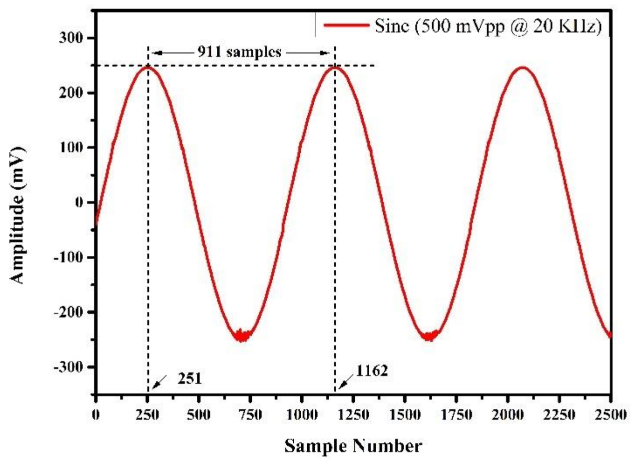

Fig. 2.38 – Sine Wave (500 mV_{pp} at 20 KHz) captured using proposed DAQ

Fig. 2.38 shows a sine wave of amplitude 500 mV_{PP} and 20 KHz frequency given from a function generator (RIGOL DG1022) and captured using the proposed DAQ system. A total of 2500 samples of the signal have been captured. For calculating the sampling interval, the 'distance between two maxima/minima' method is used. It is known that the first and second maxima occur at sample numbers 251 and 1162 respectively. That means there are a total of 911 sampling intervals between the first and second maxima. It is also known that the frequency of the sine wave is 20 KHz. Thus, the time period of the above signal, or distance between two maxima will be 50 µs. Therefore, the sampling interval of the microcontroller is (50 µs)/911 ≈ 54.88 ns.

Chapter 3

Discussion and Results

This chapter shows and discusses all the results of the experiments done on the prototypes developed (discussed in Chapter 2), and finally shows the correct acquisition of a photoacoustic signal, which was in fact the main aim of this thesis project.

3.1 Amplification of Signals

In Fig. 3.1, the working of the proposed pre-amplifier circuit can be verified. The red signal is the input sine wave (4 mV_{PP} at 1 MHz) from a function generator (RIGOL DG1022). The green signal is the amplified output of the proposed pre-amplifier circuit.

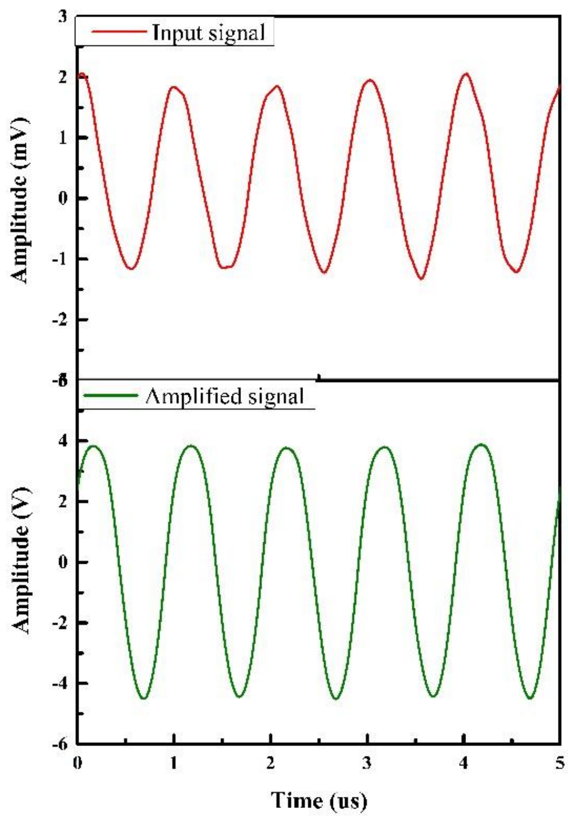

Fig. 3.1 – Input signal and its corresponding amplified signal from pre-amplifier

From the data obtained, it is known that the peak-to-peak amplitude of the output sine wave is approximately 8.6 V. Therefore, the gain of the proposed amplifier will be 8.6/0.004 = 2149.755 or 66.65 dB.

3.2 Clock Purification using CPC-P1

Figures 3.2-3.6 show the comparison between the clock generated using the microcontroller and the clock after purifying it using the clock purification circuit prototype 1 (Fig. 2.18). It can be observed that the microcontroller-generated clock has undesirable overshoots and undershoots on its rising and falling edges respectively. Amplitude degradation can also be observed at 20 MHz (Fig. 3.6).

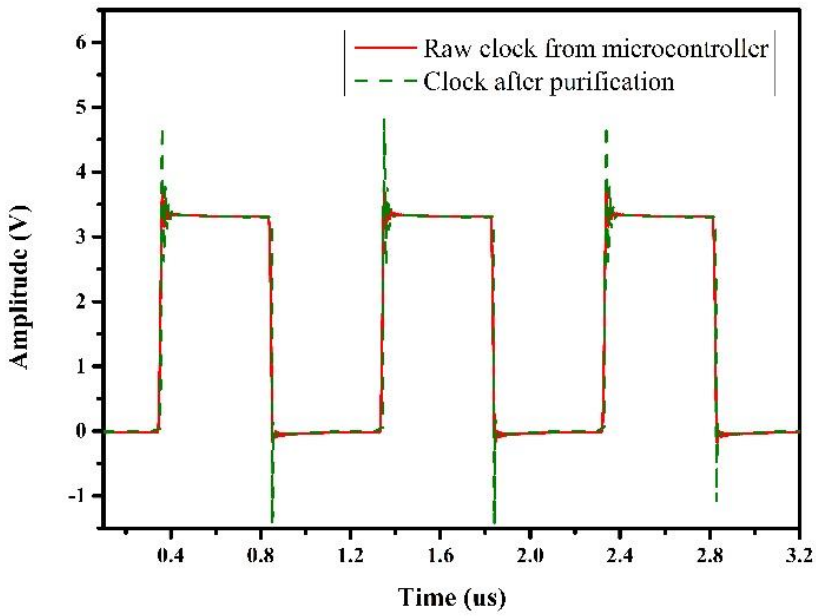

Fig. 3.2 – 1 MHz clock purified using CPC-P1

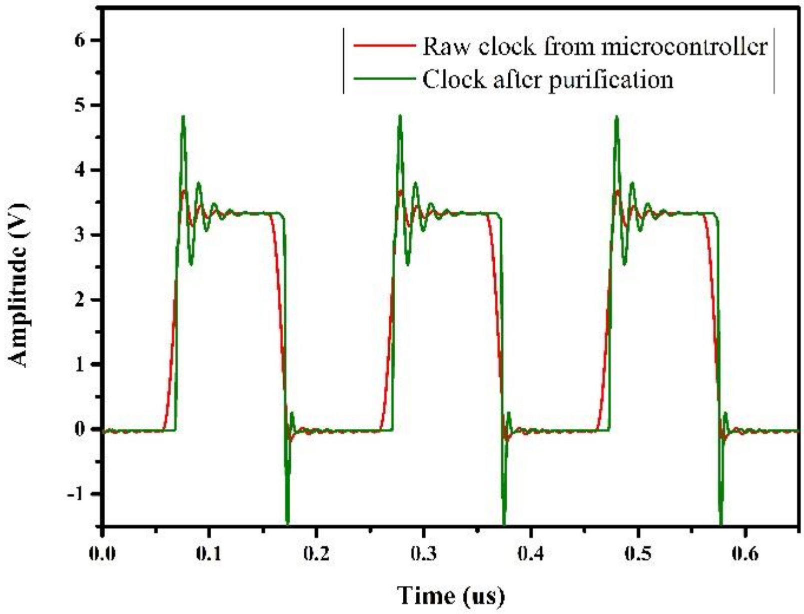

Fig. 3.3 – 5 MHz clock purified using CPC-P1

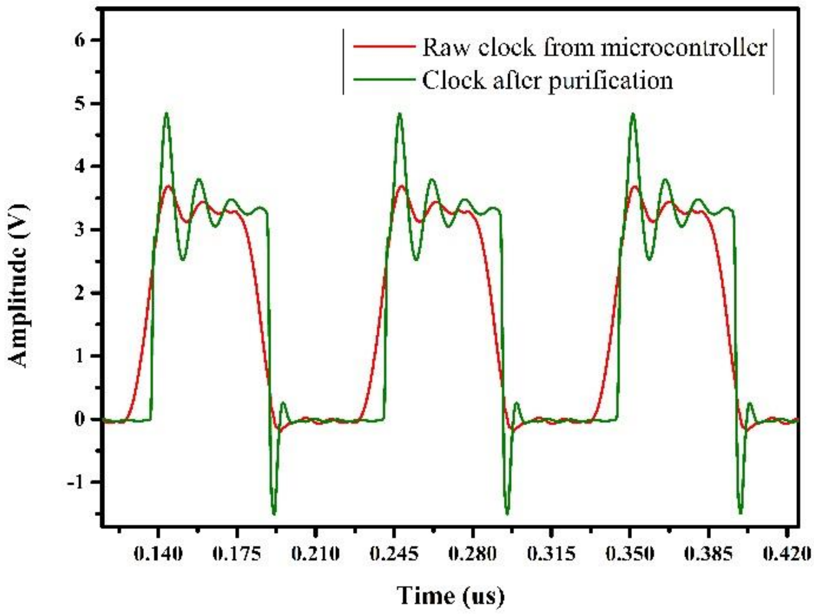

Fig. 3.4 – 10 MHz clock purified using CPC-P1

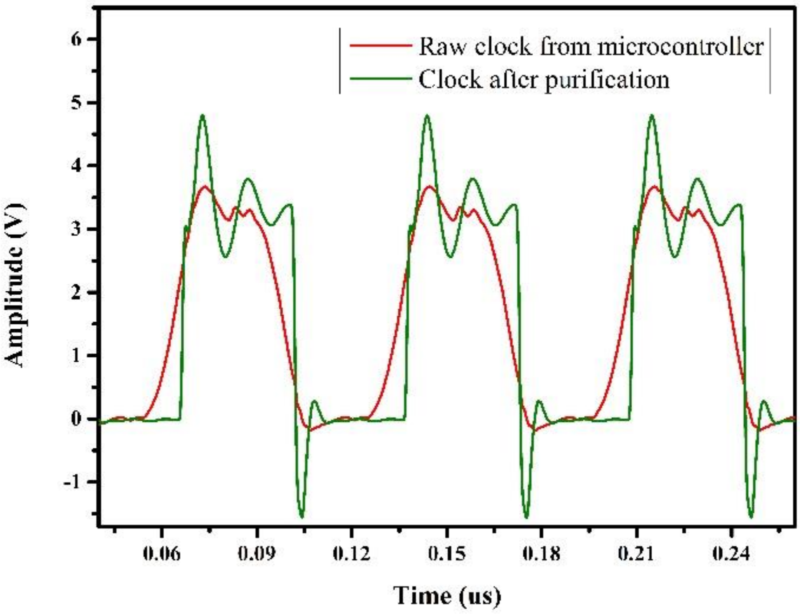

Fig. 3.5 – 14 MHz clock purified using CPC-P1

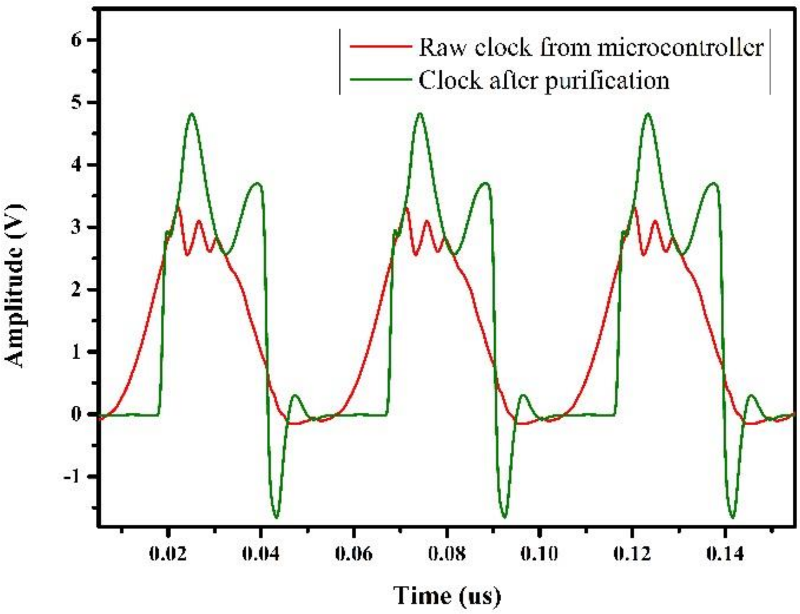

Fig. 3.6 – 20 MHz clock purified using CPC-P1

Although amplitude has been restored by the purifying circuit, but the purified clock shows even greater overshoots and undershoots. It is therefore concluded that the circuit shown in Fig. 2.18 was not able to purify the clock and thus, the next prototype circuit was designed and tested, the results of which is shown in the next section.

3.3 Clock Purification using CPC-P2

Figures 3.7-3.11 show the comparison between the clock generated using the microcontroller and the clock after purifying it using the clock purification circuit prototype 2 (Fig. 2.23). It can be observed that although the microcontroller-generated clock does not have significant overshoots/undershoots, amplitude degradation can still be observed at 20 MHz (Fig. 3.11).

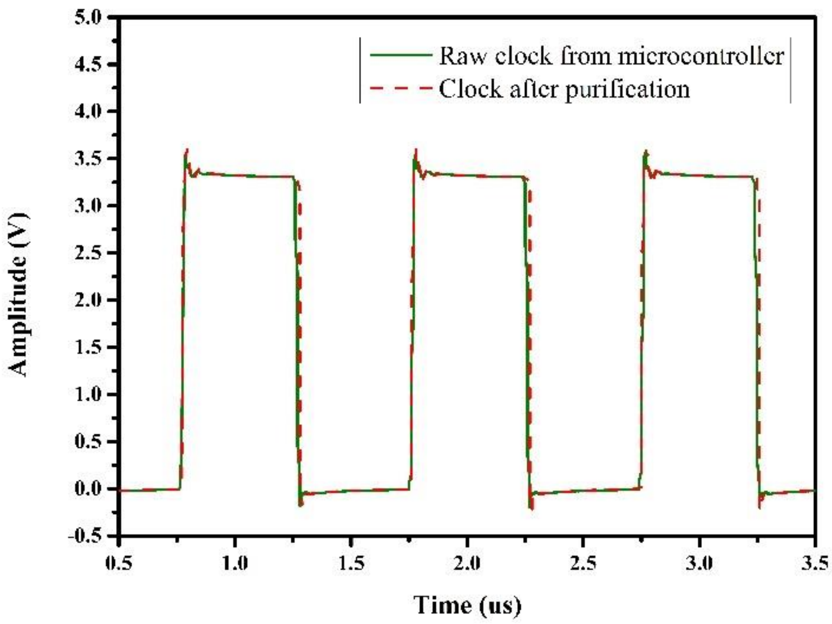

Fig. 3.7 – 1 MHz clock purified using CPC-P2

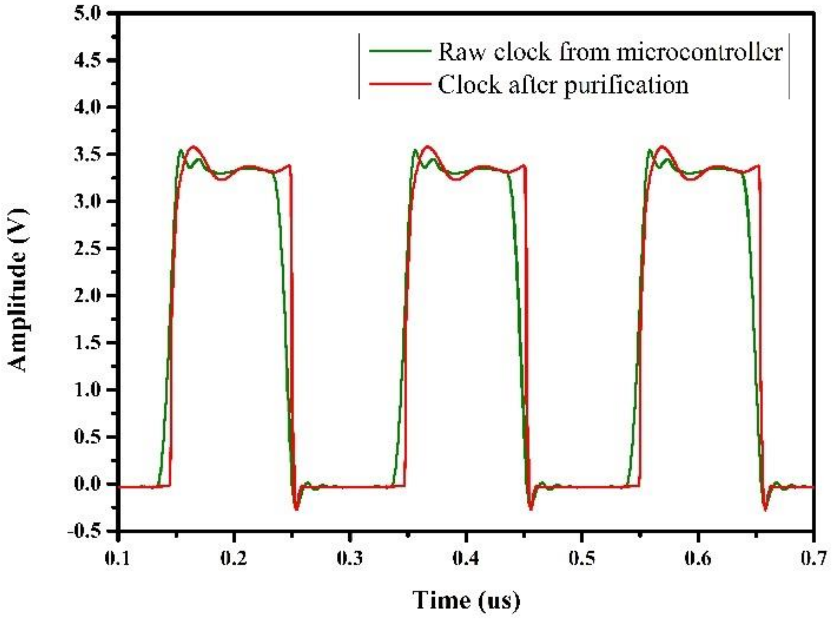

Fig. 3.8 – 5 MHz clock purified using CPC-P2

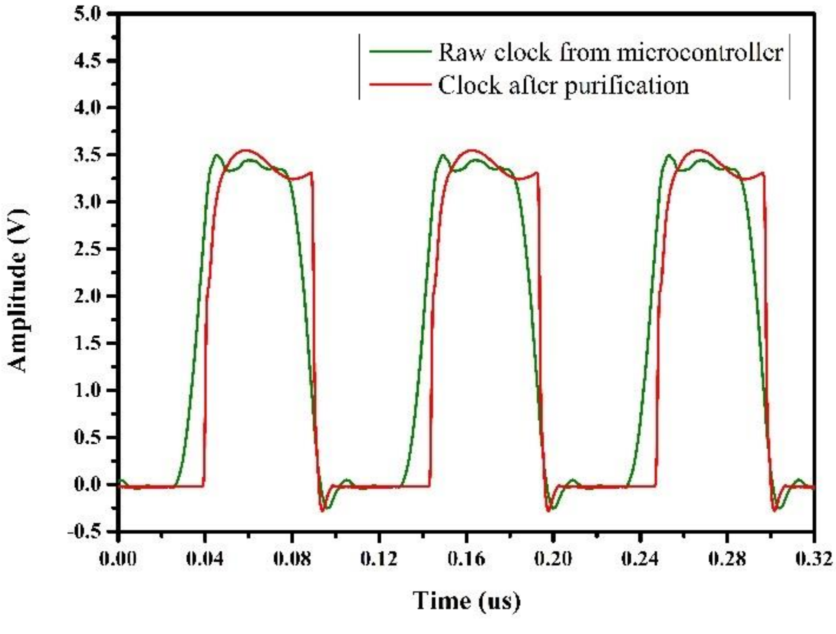

Fig. 3.9 – 10 MHz clock purified using CPC-P2

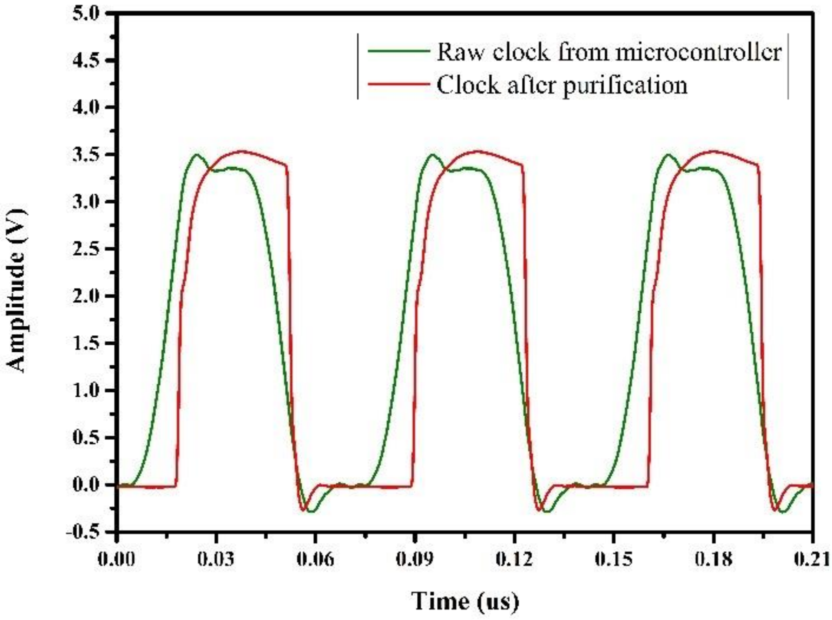

Fig. 3.10 – 14 MHz clock purified using CPC-P2

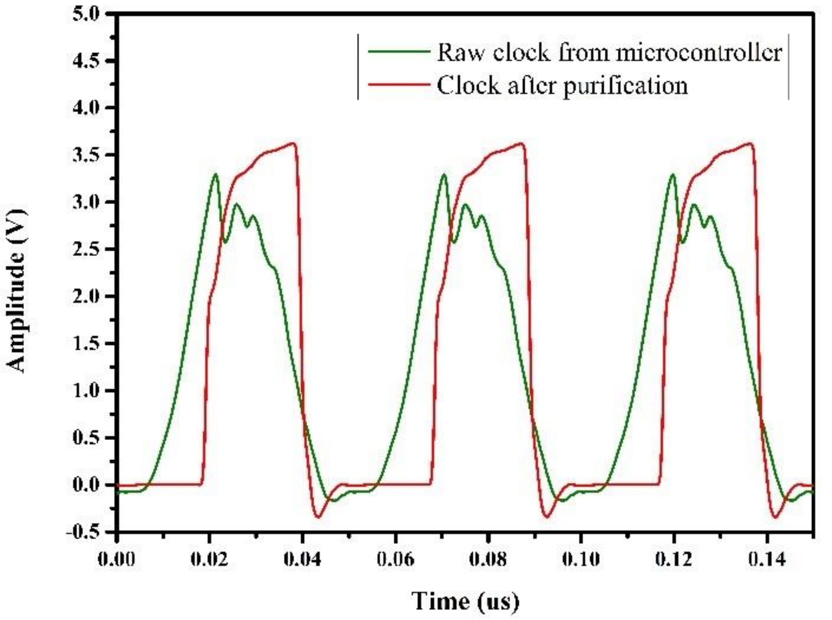

Fig. 3.11 – 20 MHz clock purified using CPC-P2

Although amplitude has been restored by the purifying circuit and also overshoots/undershoots have reduced, but an instability of the voltage threshold reference was observed at frequencies greater than 18 MHz. It is therefore concluded that although the circuit shown in Fig. 2.23 was able to purify the clock, but purification is limited to clocks having a frequency of 18 MHz or less. Thus, the next prototype circuit was designed and tested for even better results, which are shown in the next section.

3.4 Results of DAQ – prototype 1

3.4.1 Final clock purification

Figures 3.12-3.17 show the comparison between the clock generated using the microcontroller and the clock after purifying it using the clock purification circuit of DAQ prototype 1 (Fig. 2.28). It can be observed that although the microcontroller-generated clock does not have significant overshoots/undershoots, amplitude degradation can still be observed at frequencies 20 MHz (Fig. 3.16) and 26 MHz (Fig. 3.17).

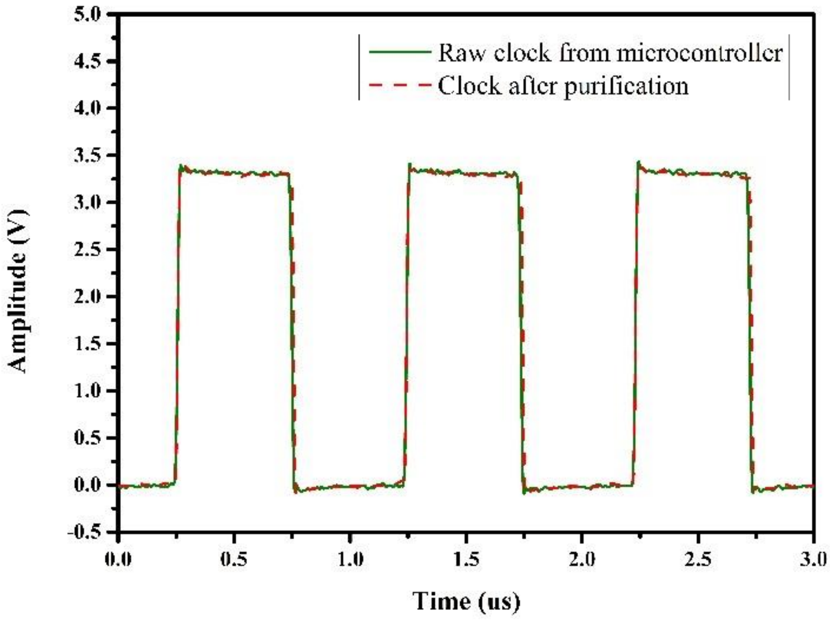

Fig. 3.12 – 1 MHz clock purified using DAQ – prototype 1

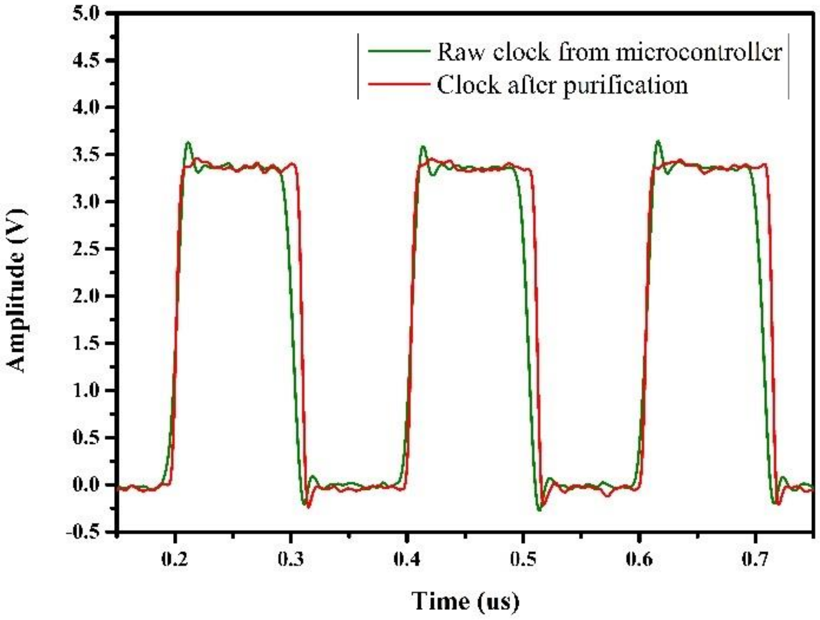

Fig. 3.13 – 5 MHz clock purified using DAQ – prototype 1

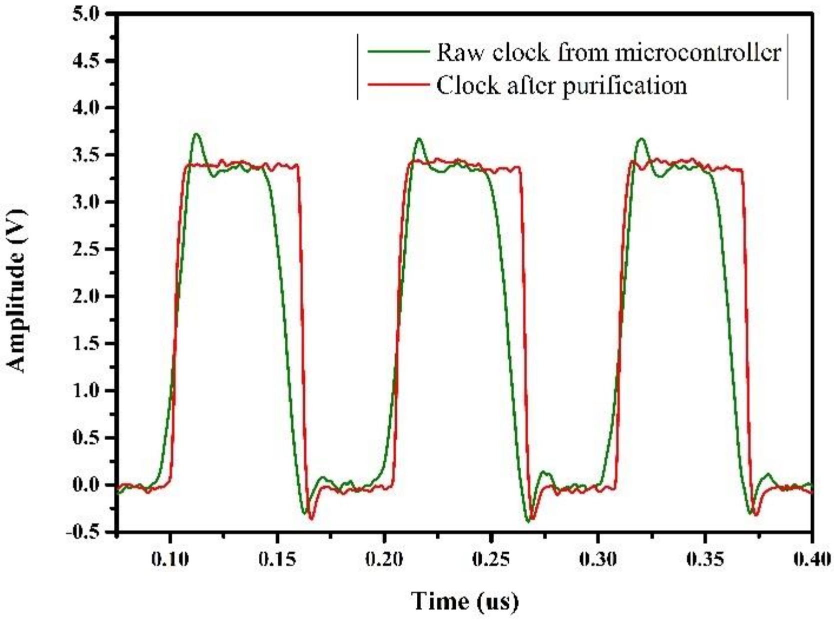

Fig. 3.14 – 10 MHz clock purified using DAQ – prototype 1

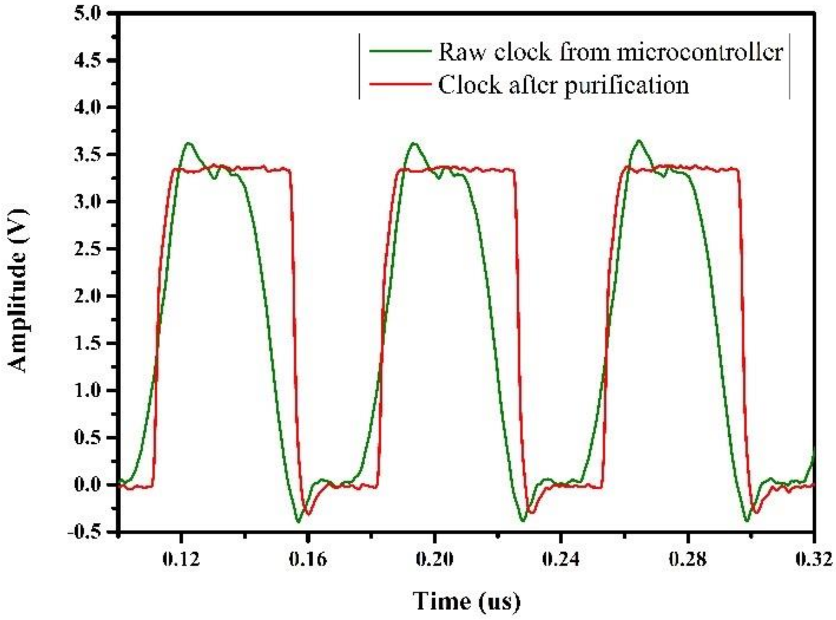

Fig. 3.15 – 14 MHz clock purified using DAQ – prototype 1

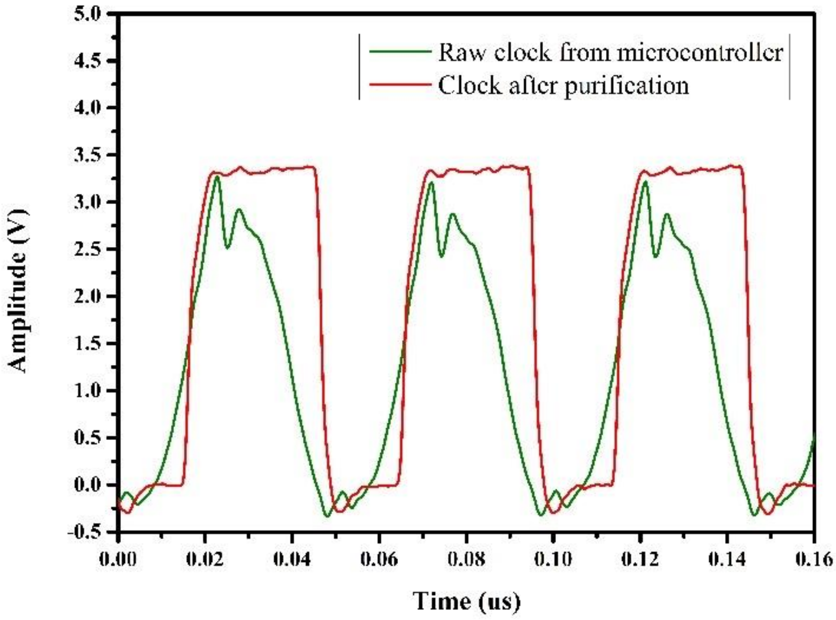

Fig. 3.16 – 20 MHz clock purified using DAQ – prototype 1

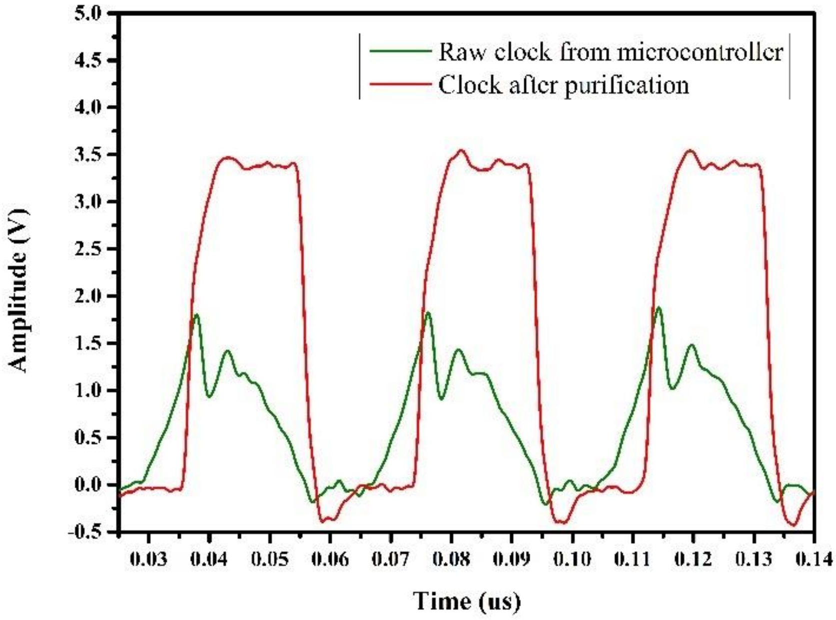

Fig. 3.17 – 26 MHz clock purified using DAQ – prototype 1

By observing figures 3.12-3.17, it can be concluded that the circuit shown in Fig. 2.28 is able to reduce the amount of overshoots/undershoots and also compensate for any amplitude degradation in the clock.

3.4.2 Trigger signal restoration

Figure 3.18 shows the comparison between the trigger signal coming from the LASER setup and the trigger signal after purifying it using the trigger signal restoration circuit of DAQ prototype 1 (Fig. 2.28). The 'HIGH' voltage level of the trigger from the LASER is 1.5V which is not sufficient to trigger the microcontroller. Therefore, it is passed through a comparator circuit to boost the voltage to 3.3V, which is shown in Fig. 3.18.

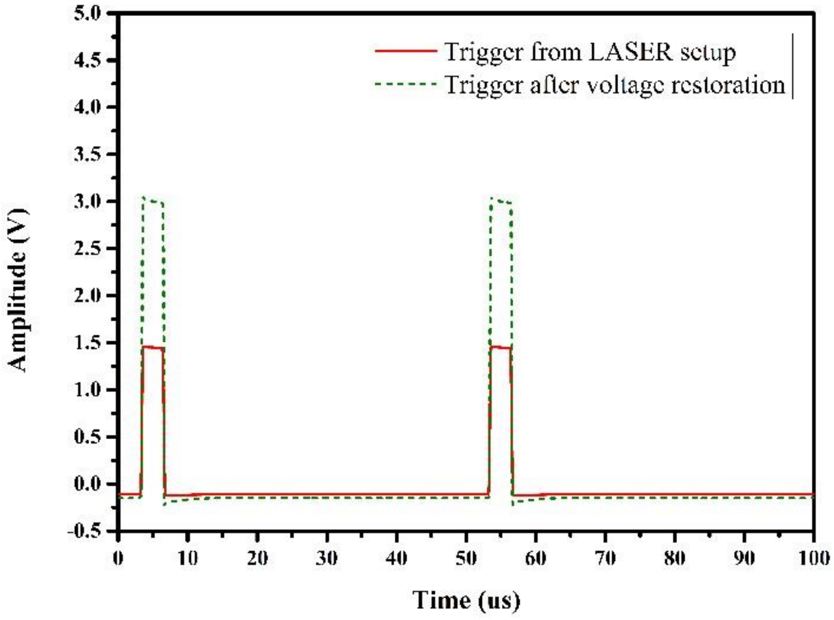

Fig. 3.18 – 20 KHz trigger coming from the laser setup before and after purification

3.4.3 Acquisition of sine wave

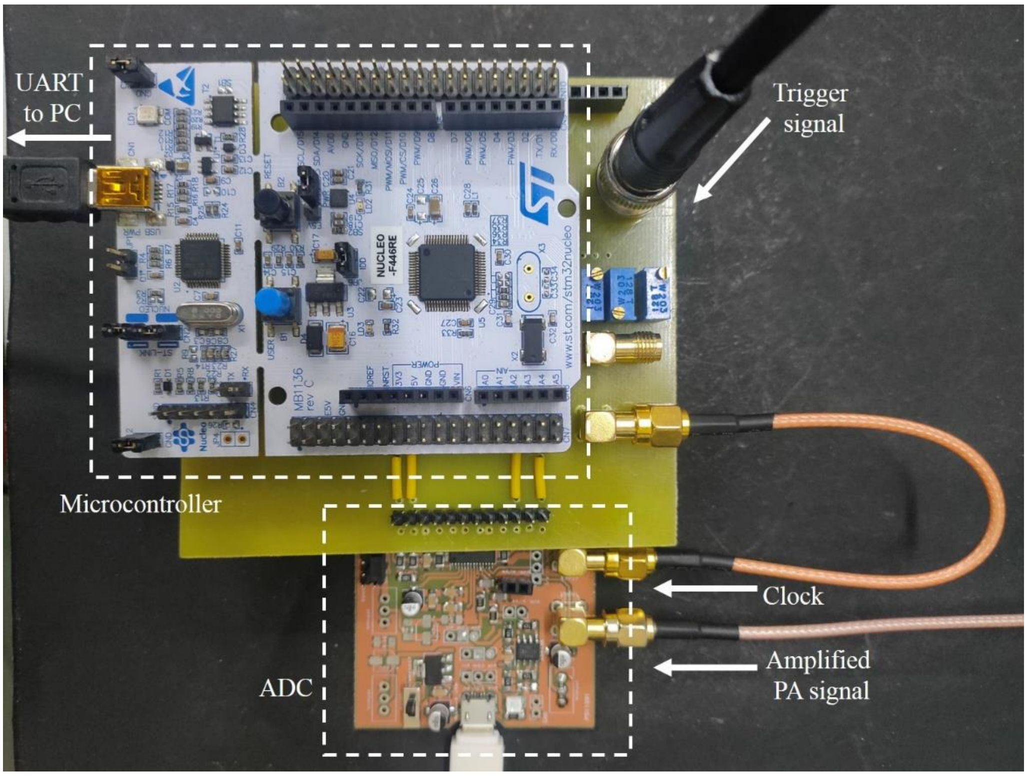

Fig. 3.19 – Assembled setup for acquisition of data using the proposed DAQ

Fig. 3.19 shows the assembled experimental setup of the proposed DAQ. This setup is used to acquire different signals. At the bottom center of Fig. 3.19, the digital output of the ADC is supposed to be connected to the microcontroller. Three ADC module PCBs with different specifications were developed in this thesis. The specifications of them are as follows: -

- ADC-1 – AD9215 (10-bit resolution) has been used in this module. The analog input range has been set to 2 V_{PP}. This results in a step size of 1.955 mV.
- ADC-2 – AD9215 (10-bit resolution) has been used in this module. The analog input range has been set to 1 V_{PP}. This results in a step size of 0.977 mV.
- ADC-3 – AD9235 (12-bit resolution) has been used in this module. The analog input range has been set to 1 V_{PP}. This results in a step size of 0.244 mV.

Fig. 3.20 shows the comparison between the three developed ADCs. For reference, a 500 KHz, 30 mV_{PP} (-15 mV to +15 mV) sine wave from a function generator (RIGOL DG1022) was acquired using the proposed DAQ by connecting the three developed ADCs. The acquired sine waves are shown in Fig. 3.20. ADC-1 shows considerable distortion in the acquired signal. Thus, ADC-1 was found not suitable for acquisition of signals. ADC-2 and ADC-3 show satisfactory results, since no distortion is observed in the signals acquired using these two ADCs. Both ADC-2 and ADC-3 can be used for acquisition of signals by connecting them to the proposed DAQ.

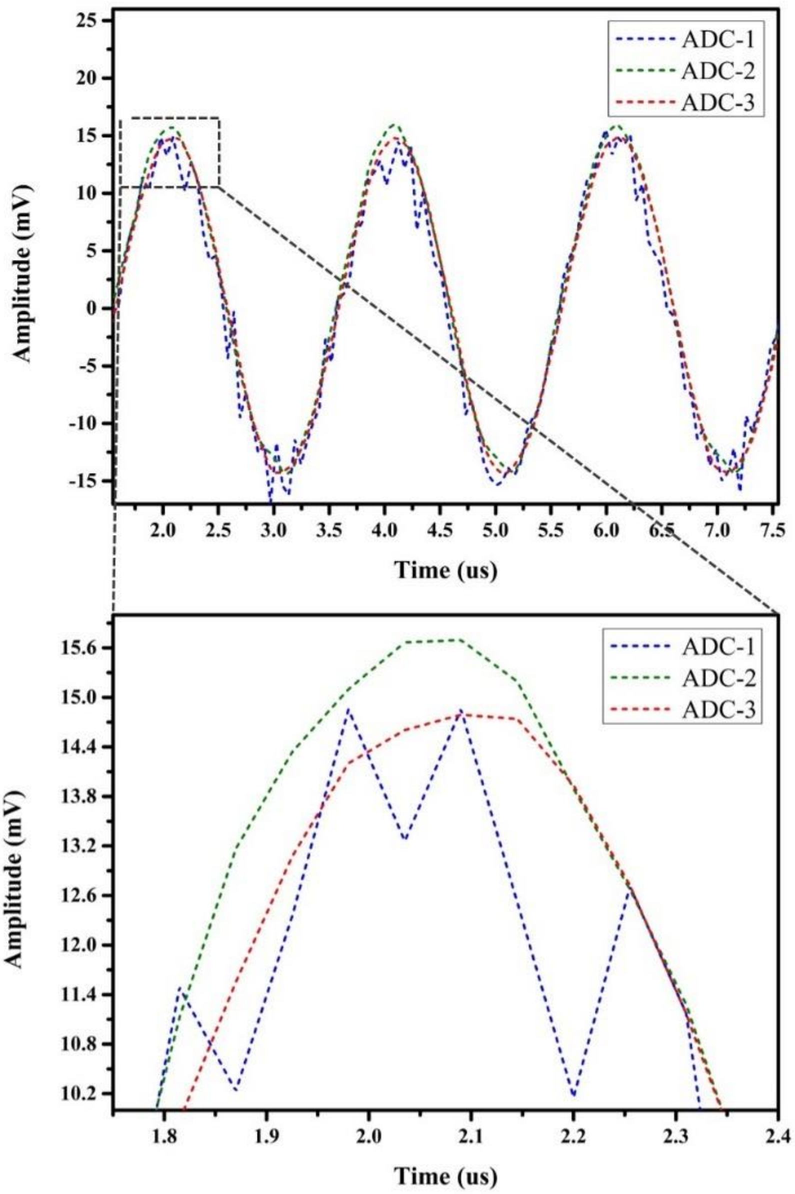

Fig. 3.20 – Sine wave (30 mV_{PP} at 500 KHz) acquired using all three ADC prototypes

Parameter	**ADC – 1**	**ADC – 2**	**ADC – 3**
Step size	1.955 mV	0.977 mV	0.244 mV
Peak to Peak amplitude	35.64 mV	31.35 mV	29.88 mV
Error %	18.8%	4.5%	0.4%

Table 3.1 – Comparison of ADC prototypes

The comparison of results between the three ADCs is shown in Table 3.1. It can be clearly understood that lesser the step-size, smoother the signal. ADC-3 has the lowest step-size of 0.244 mV and hence has the smoothest acquisition of the sine wave compared to the other two ADCs. The observed peak-to-peak amplitude of the sine waves acquired have also been mentioned in Table 3.1. An error% of 0.4% is observed when the signal is acquired using ADC-3, which is the lowest among all three prototypes developed. Hence, ADC-3 was finally chosen to be used for further experiments and acquisition of PA signals.

Fig. 3.21 shows three sine waves (500 KHz) of different amplitudes acquired using ADC-3. The sine waves are given from a function generator (RIGOL DG1022). Accurate acquisition of signals was observed for all three amplitudes. It can thus be concluded that the proposed DAQ is able to accurately acquire signals of different amplitudes.

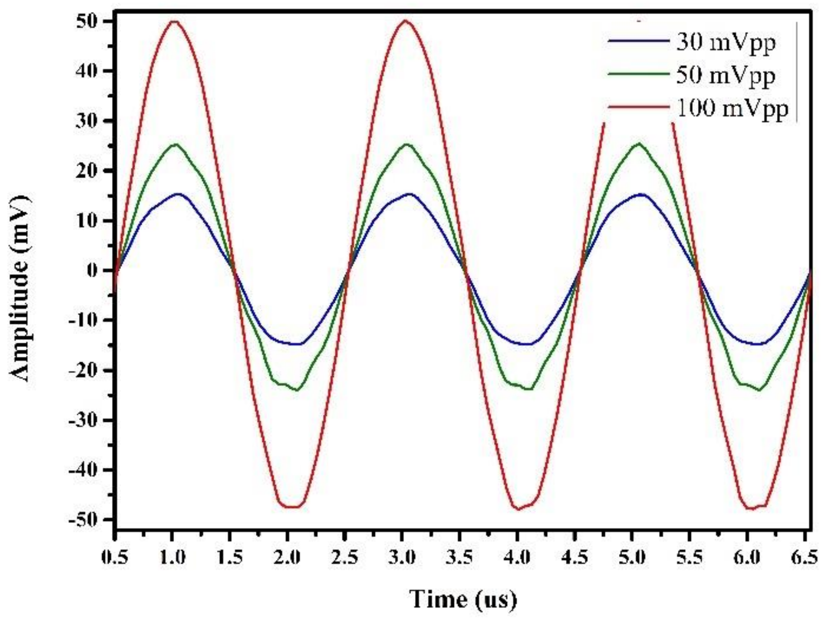

Fig. 3.21 – Sine wave (500 KHz) acquired at varying amplitude using ADC-3 prototype

Fig. 3.22 shows three sine waves (30 mV_{PP}) at different frequencies acquired using ADC-3. The sine waves are given from a function generator (RIGOL DG1022). Accurate acquisition of signals was observed for all three frequencies. It can thus be concluded that the proposed DAQ is able to accurately acquire signals at different frequencies even in the MHz range.

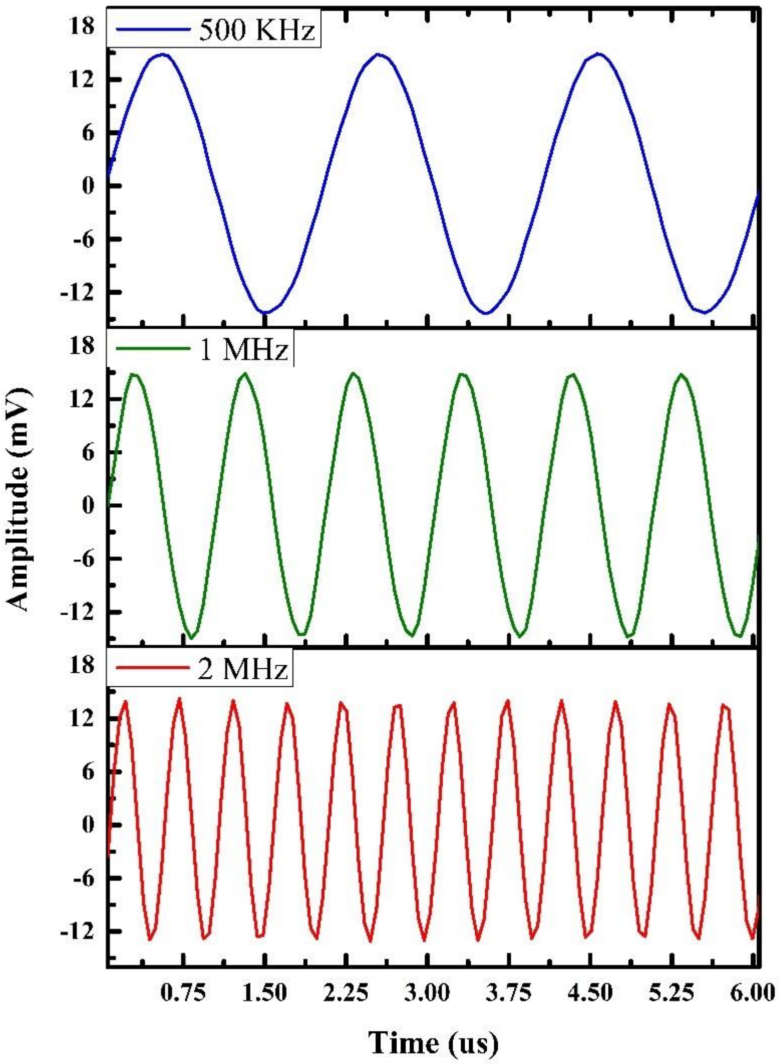

Fig. 3.22 – Sine wave (30 mV_{PP}) acquired at varying frequency using ADC-3 prototype

3.4.4 Acquisition of PA signals

In Section 3.4.3, a proof-of-concept study of the proposed DAQ was done, to show that accurate acquisition of known signals (with varying parameters) can be done using the proposed DAQ. The acquisition of PA signals was performed, which was the main aim of this thesis project. A custom-built laser diode-based excitation system was used in a photoacoustic imaging experimentation setup, to excite a black rubber sample. The voltage from the high-voltage power supply was set to 100V. The emitted ultrasound waves were captured by the ultrasound transducer. This PA signal was passed through the proposed pre-amplifier circuit. The output of amplifier was given to the conventional DSO and the proposed DAQ simultaneously. The amplified PA signals captured through the DSO and DAQ are shown in Fig. 3.23. The peak-to-peak PA amplitude of the DSO is 34.48 mV_{PP}, whereas the peak-to-peak PA amplitude of the DAQ is 34.67 mV_{PP}. This proves that the proposed DAQ can be used to successfully acquire PA signals, as a replacement to the traditional signal capturing instrument i.e., DSO.

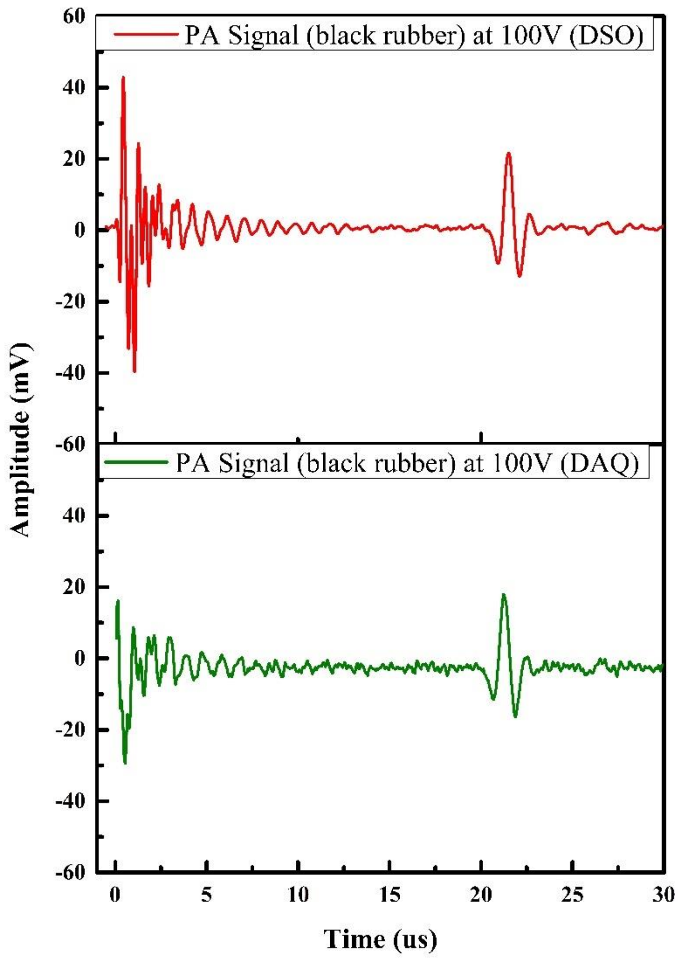

Fig. 3.23 – PA signal (at 100V input) acquired using DSO and proposed DAQ (with ADC-3)

To justify the sensitivity of the proposed DAQ, the voltage from the high-voltage power supply was increased to 150V and the PA sensing experiment was repeated. The acquired PA signal is shown in Fig. 3.24. The peak-to-peak PA amplitude of the DAQ is 81.2 mV. By increasing the excitation voltage, a proportional increase in the peak-to-peak amplitude of the PA signal can be observed.

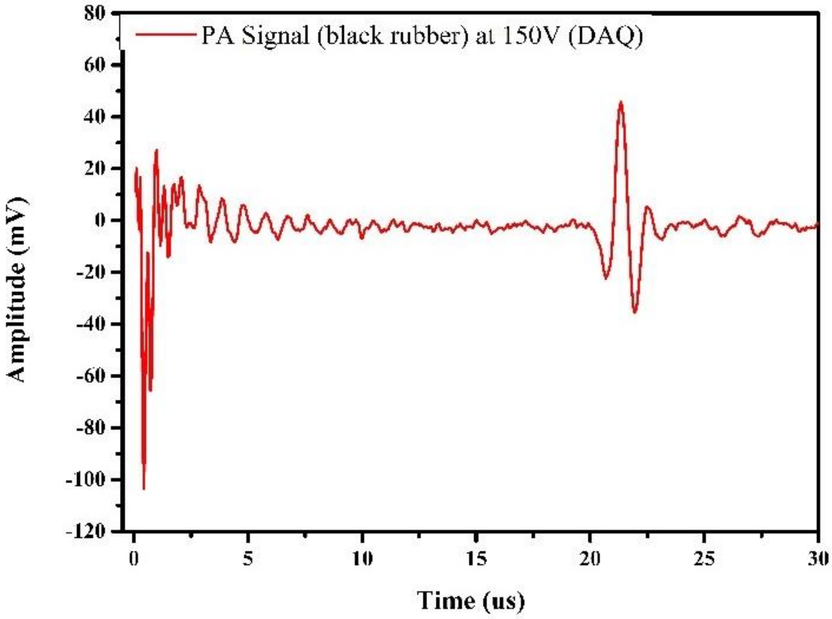

Fig. 3.24 – PA signal (at 150V input) acquired using proposed DAQ (with ADC-3)

Chapter 4

Conclusion and Future Scope

In this thesis, a novel data acquisition system (DAQ) has been developed to read and store photoacoustic signals. The key motivation behind building a data acquisition system is to replace the traditional signal capturing instruments like the DSOs. The two main problems in acquiring PA signals are that they lie in the 3-20 MHz spectrum and the signal amplitude is in the range of tens of microvolts. Both these issues, along with other minor issues have been addressed in this thesis.

Initially, the core problem has been divided into smaller blocks and have been dealt with and solved individually. The first task is to amplify the low-amplitude PA signals. This has been done by passing the signal through a pre-amplifier circuit of gain 66.65 dB. The amplified PA signals is then digitized by passing it through a high-frequency, high resolution, precision 12-bit ADC. The ADC circuit was designed carefully after several experimentations and three prototype PCBs developed for the same. After digitization of the signal, it is read by a microcontroller. Parallel reading of all 12-bits has been ensured to achieve true high-frequency acquisition. The microcontroller has also been used to generate a high-frequency clock for the ADC. Overshoots, undershoots and amplitude degradation are observed at clock frequencies exceeding 15 MHz. Therefore, a clock purification circuit has also been included in the system. Also, in order to eliminate the noise accompanying the PA signal, time-averaging method is used. To achieve that, the same signal needs to be acquired multiple times synchronously. For synchronization, the laser setup is generating a trigger signal when the laser is incident upon the sample. This trigger signal (after boosting its voltage) is given as an interrupt to the microcontroller, to ensure acquisition only when the sample is excited by the laser.

The proposed DAQ system is this thesis was developed and thoroughly tested to verify its operation to acquire PA signals. But this does not mean that there is no room for improvement and modification. The sample used in this thesis to conduct PA imaging experiments is black rubber. The ultimate application for the proposed DAQ would be to acquire the PA signals generated upon excitation of laser onto live or cancerous human tissues. The frequency and amplitude of tissue would obviously be different from black rubber sample. In the future, the samples might be analysed, and accordingly the DAQ may be calibrated. This may include altering the gain of the amplifier or increasing the resolution and sampling rate of the ADC and microcontroller. The DAQ developed is application-specific and calibrated according to the need i.e., acquiring photoacoustic signals. But the system may be modified for any other application, according to the system's specifications. To increase the specifications of the proposed DAQ, different hardware could be explored, incorporated in the proposed block diagram and then tested to verify its functioning.

The kind of DAQ developed is a low-cost and compact one. Upon extensive research, experiments and data collection, this project might be very useful for developing portable, handheld biomedical instruments. By incorporating the proposed DAQ in a custom-built laser excitation system, a complete PA imaging-based cancer diagnosis instrument can be developed, which could serve as a low-cost, safe and viable replacement of existing imaging techniques like MRI, CT scan, etc.

References

[1] Jiang, Daohuai, Yifei Xu, Yongjian Zhao, Hengrong Lan, and Fei Gao. "Low-Cost Photoacoustic Tomography System Based on Water- Made Acoustic Delay-Line." In 2019 IEEE International Ultrasonics Symposium (IUS), pp. 2369-2372. IEEE, 2019.

[2] Mahzan, N. N., et al. "Design and development of an arduino based data logger for photovoltaic monitoring system." Int. J. Simul. Syst. Sci. Technol 17.41 (2017): 15-1.

[3] González, Alejandro, José Luis Olazagoitia, and Jordi Vinolas. "A low-cost data acquisition system for automobile dynamics applications." Sensors 18.2 (2018): 366.

[4] Salgado, Débora Pereira, et al. "A QoE assessment method based on EDA, heart rate and EEG of a virtual reality assistive technology system." Proceedings of the 9th ACM Multimedia Systems Conference. 2018.

[5] Rosencwaig A. and Peter R. Griffiths. "Photoacoustics and photoacoustic spectroscopy." *Physics Today* 34.6 (1981): 64.

[6] Valluru, Keerthi S., Bhargava K. Chinni, Navalgund A. Rao, Shweta Bhatt, and Vikram S. Dogra. "Basics and clinical applications of photoacoustic imaging." Ultrasound Clinics 4, no. 3 (2009): 403-429.

[7] Manohar, Srirang, and Daniel Razansky. "Photoacoustics: a historical review." Advances in optics and photonics 8, no. 4 (2016): 586-617.

[8] Upputuri, Paul K., and Manojit Pramanik. "Recent advances toward preclinical and clinical translation of photoacoustic tomography: a review." *Journal of biomedicaloptics* 22.4 (2016): 041006.

[9] Wang, Lihong V., and Hsin-I. Wu. Biomedical optics: principles and imaging. John Wiley & Sons, 2012.

[10] Beard, Paul. "Biomedical photoacoustic imaging." Interface Focus 1, no. 4 (2011): 602-631.

[11] C. Zhang and Y. Wang, "Comparison of Various Imaging Modes for Photoacoustic Tomography", in 13th International Conference on

Biomedical Engineering, Springer, Berlin, Heidelberg, 2009, pp. 121– 124.

[12] Wang, Sheng, et al. "Recent advances in photoacoustic imaging for deep-tissue biomedical applications." *Theranostics* 6.13 (2016): 2394.

[13] Bell, Alexander Graham. "On the production and reproduction of sound by light." *Proc. Am. Assoc. Adv. Sci.*. Vol. 29. 1881.

[14] De Montigny, Etienne. "Photoacoustic Tomography: Principles and applications." Department of Physics Engineering, polytechnic school Montreal (2011).

[15] Kratkiewicz, Karl, et al. "Technical considerations when using verasonics research ultrasound platform for developing a photoacoustic imaging system." *arXiv preprint arXiv:2008.06086* (2020).

[16] Daniel J Bell(2020) Ultrasound Transducer. RadioPaedia. https://radiopaedia.org/articles/ultrasound-transducer. Accessed 22 April 2022

[17] Wallyn, Justine, et al. "Biomedical imaging: principles, technologies, clinical aspects, contrast agents, limitations and future trends in nanomedicines." *Pharmaceutical Research* 36.6 (2019): 1-31.

[18] Maslov, Konstantin, Hao F. Zhang, Song Hu, and Lihong V. Wang. "Optical-resolution photoacoustic microscop1y for in vivo imaging of single capillaries." Optics Letters 33, no. 9 (2008): 929-931.

[19] Wang, Lihong V. "Tutorial on photoacoustic microscopy and computed tomography." IEEE Journal of Selected Topics in Quantum Electronics 14, no. 1 (2008): 171-179.

[20] Zou, Chunpeng, et al. "Biomedical photoacoustics: fundamentals, instrumentation and perspectives on nanomedicine." *International journal of nanomedicine* 12 (2017): 179.

[21] Van de Sompel, Dominique, et al. "Improving image quality by accounting for changes in water temperature during a photoacoustic tomography scan." (2012): e45337.

[22] Neuschmelting, Volker, et al. "Performance of a multispectral optoacoustic tomography (MSOT) system equipped with 2D vs. 3D handheld probes for potential clinical translation." *Photoacoustics* 4.1 (2016): 1-10.

[23] Kuniyil Ajith Singh, Mithun, Wiendelt Steenbergen, and Srirang Manohar. "Handheld probe-based dual mode ultrasound/photoacoustics for biomedical imaging." *Frontiers in Biophotonics for Translational Medicine*. Springer, Singapore, 2016. 209-247.

[24] Tian, Chao, et al. "Impact of system factors on the performance of photoacoustic tomography scanners." *Physical Review Applied* 13.1 (2020): 014001.

[25] Doug Mercer (2021) Analog to Digital Conversion. Analog Devices. https://wiki.analog.com/university/courses/electronics/text/chapter-20. Accessed 29 April 2022

[26] Grant Maloy Smith (2020) Types of A/D Converters – The Ultimate Guide. Dewesoft. https://dewesoft.com/daq/types-of-adc-converters. Accessed 02 May 2022

[27] Shu, Shuangbao, et al. "A high-speed data acquisition system based on FPGA for tokamak." *Review of Scientific Instruments* 89.10 (2018): 10K120.

[28] STM32F446RE – Datasheet. STMicroelectronics. https://www.st.com/resource/en/datasheet/stm32f446re.pdf. Accessed 05 May 2022

[29] NUCLEO – 446RE. element14. https://au.element14.com/stmicroelectronics/nucleo-f446re/dev-board-arduino-mbed-nucleo/dp/2491978. Accessed 02 May 2022

[30] González, Alejandro, José Luis Olazagoitia, and Jordi Vinolas. "A low-cost data acquisition system for automobile dynamics applications." *Sensors* 18.2 (2018): 366.

[31] Nhivekar, G. S., and R. R. Mudholker. "Data Logger and Remote Monitoring System for Multiple Parameter Measurement Applications." *e-Journal of Science & Technology* 6.3 (2011).

[32] Gakopoulos, Sotirios, et al. "Development of a data logger for capturing human-machine interaction in wheelchair head-foot steering sensor system in dyskinetic cerebral palsy." *Sensors* 19.24 (2019): 5404.

[33] Dantsker, Or D., et al. "High-frequency sensor data acquisition system (SDAC) for flight control and aerodynamic data collection." *32nd AIAA Applied Aerodynamics Conference*. 2014.

[34] Soto-Ocampo, César Ricardo, et al. "Low-cost, high-frequency, data acquisition system for condition monitoring of rotating machinery through vibration analysis-case study." *Sensors* 20.12 (2020): 3493.

[35] Srivathsan Vasudevan, K. Harishwar Reddy (2021) Data Acquisition System for Photoacoustic Systems. DSpace IITI. http://dspace.iiti.ac.in:8080/jspui/handle/123456789/3058. Accessed 24 April 2022.

[36] AD9283 – Datasheet. Analog Devices. https://www.analog.com/media/en/technical-documentation/data-sheets/ad9283.pdf. Accessed 05 May 2022

[37] AD9215 – Datasheet. Analog Devices. https://www.analog.com/media/en/technical-documentation/data-sheets/ad9215.pdf. Accessed 05 May 2022

[38] AD9235 – Datasheet. Analog Devices. https://www.analog.com/media/en/technical-documentation/data-sheets/ad9235.pdf. Accessed 05 May 2022

[39] AD9244 – Datasheet. Analog Devices. https://www.analog.com/media/en/technical-documentation/data-sheets/ad9244.pdf. Accessed 05 May 2022

[40] RS Components India. https://in.rsdelivers.com/. Accessed 24 May 2022)